



## Design and synthesis of novel 3,5-bis-*N*-(aryl/heteroaryl) carbamoyl-4-aryl-1,4-dihydropyridines as small molecule BACE-1 inhibitors



Nima Razzaghi-Asl<sup>a</sup>, Omidreza Firuzi<sup>a</sup>, Bahram Hemmateenejad<sup>a,c</sup>, Katayoun Javidnia<sup>a,b</sup>, Najmeh Edraki<sup>a</sup>, Ramin Miri<sup>a,b,\*</sup>

<sup>a</sup> Medicinal and Natural Products Chemistry Research Center, Shiraz University of Medical Sciences, PO Box 3288-71345, Shiraz, Iran

<sup>b</sup> Department of Medicinal Chemistry, Faculty of Pharmacy, Shiraz University of Medical Sciences, PO Box 3288-71345, Shiraz, Iran

<sup>c</sup> Chemistry Department, Shiraz University, Shiraz, Iran

### ARTICLE INFO

#### Article history:

Received 8 July 2013

Revised 4 September 2013

Accepted 12 September 2013

Available online 20 September 2013

#### Keywords:

Alzheimer

BACE-1

Dihydropyridine

Virtual screening

### ABSTRACT

Alzheimer disease (AD) is a neuronal dementia for which no treatment has been consolidated yet. Major pathologic hallmark of AD is the aggregated extracellular amyloid- $\beta$  plaques in the brains of disease sufferers. A $\beta$ -peptide is a major component of amyloid plaques and is produced from amyloid precursor protein (APP) via the proteolysis action. An aspartyl protease known as  $\beta$ -site amyloid precursor protein cleaving enzyme (BACE-1) is responsible for this proteolytic action. Distinctive role of BACE-1 in AD pathogenesis has made it a validated target to develop anti-Alzheimer agents. Our structure-based virtual screening method led to the synthesis of novel 3,5-bis-*N*-(aryl/heteroaryl) carbamoyl-4-aryl-1,4-dihydropyridine BACE-1 inhibitors (**6a–6p**; *in vitro* hits). Molecular docking and DFT-based *ab initio* studies using B3LYP functional in association with triple- $\zeta$  basis set (TZV) proposed binding mode and binding energies of ligands in the active site of the receptor. *In vitro* BACE-1 inhibitory activities were determined by enzymatic fluorescence resonance energy transfer (FRET) assay. Most of the synthesized dihydropyridine scaffolds were active against BACE-1 while **6d**, **6k**, **6n** and **6a** were found to be the most potent molecules with IC<sub>50</sub> values of 4.21, 4.27, 4.66 and 6.78  $\mu$ M, respectively. Superior BACE-1 inhibitory activities were observed for dihydropyridine derivatives containing fused/nonfused thiazole containing groups, possibly attributing to the additional interactions with S2–S3 subpocket residues. Relatively reliable correlation between calculated binding energies and experimental BACE-1 inhibitory activities was achieved ( $R^2 = 0.51$ ). Moreover, compounds **6d**, **6k**, **6n** and **6a** exhibited relatively no calcium channel blocking activity with regard to nifedipine suggesting them as appropriate candidates for further modification(s) to BACE-1 inhibitory scaffolds.

© 2013 Elsevier Ltd. All rights reserved.

### 1. Introduction

Alzheimer disease (AD) is a neurodegenerative disorder clinically recognized by progressive decline in memory and cognition.<sup>1</sup> AD accounts for most cases of dementia in the elderly population.<sup>2,3</sup> Histological examination of the brains of affected individuals has revealed the existence of significant synaptic loss.<sup>4</sup> The main neuropathological characteristics of AD are the presence of extracellular amyloid plaques and intracellular Neurofibrillary tangles (NFT) in the brain. The amyloid plaques result from the deposition of aggregated amyloid beta (A $\beta$ ) peptides. A $\beta$  peptides (mainly as A $\beta$ <sub>40</sub> and A $\beta$ <sub>42</sub>) are the product of two consecutive proteolytic cleavages on a large trans-membrane protein; amyloid precursor protein (APP).

By 1999, various independent researchers discovered BACE-1 as the aspartyl protease  $\beta$ -site APP-cleaving enzyme. BACE-1 initiates the amyloid cascade by cleavage of APP.<sup>5,6</sup> Subsequent cleavage of the C-terminus of APP by  $\gamma$ -secretase results in the formation of A $\beta$ <sub>40</sub> and A $\beta$ <sub>42</sub>. In the nonamyloidogenic pathway,  $\alpha$ -secretase cleaves APP leading to the generation of neuroprotective peptide sAPP $\alpha$ .<sup>7</sup>

Inhibition of  $\beta$  and  $\gamma$ -secretase enzymes by small molecule blockers is a promising approach to find therapeutic agents for AD. In this regard, inhibition of  $\beta$ -secretase is very importance since several studies have shown that inhibition of  $\gamma$ -secretase may have some mechanism-based adverse effects.<sup>8,9</sup> The strategy of BACE-1 blockade for AD-therapy has been further supported by the observation of normal phenotype in BACE-1 knockout mice.<sup>10</sup>

Many research groups have focused on the development of BACE-1 inhibitors.<sup>11,12</sup> BACE-1 inhibitors were primarily designed

\* Corresponding author. Tel./fax: +98 711 2303872.

E-mail address: [miri@sums.ac.ir](mailto:miri@sums.ac.ir) (R. Miri).

mimicking the structures of substrate and transition-state analogs with sub-nanomolar activities,<sup>11</sup> but poor pharmacokinetic profile of peptidic inhibitors prevented them from being further developed to oral bioavailable CNS drugs. Recently significant numbers of BACE-1 inhibitors have been developed as small molecule candidates possessing drug-like features.<sup>3,13</sup> In this regard, a diverse set of chemical scaffolds have been proposed as BACE-1 inhibitors.<sup>14,15</sup> For more information, readers are referred to the ChEMBL database.<sup>16</sup>

Among nitrogen containing heterocycles, 1,4-dihydropyridine (DHP) is a privileged scaffold with a broad range of pharmacological activities. Several DHPs have found their way to the drug market as calcium channel blockers.<sup>17,18</sup> However, little attention has been directed towards the BACE-1 blocking activity of these compounds.<sup>19,20</sup> Choi and co-workers have reported novel *N*-methyl-sulfonamide-1,4-dihydropyridine derivatives with IC<sub>50</sub> values of 8–30 μM in a cell-based assay.<sup>19</sup>

DHPs have many features that make them privileged chemical scaffolds. They can be converted to the quaternary amines leading to their retention in the brain.<sup>21,22</sup> Another characteristic feature of DHP scaffold is the possibility of structural modifications via introducing various chemical substituents in different positions of the DHP ring and hence providing remarkable changes in pharmacological profile.<sup>19,23</sup>

In continuation to our interest in novel BACE-1 inhibitors,<sup>24</sup> and also to further extend the scope of 1,4-DHPs as privileged small molecule medicinal scaffolds,<sup>25,26</sup> we hereby report molecular modeling, synthesis, and in vitro FRET-based BACE-1 inhibitory activities of some new 2,6-dimethyl-3,5-bis-*N*-(aryl) carbamoyl-4-aryl-(aryl/heteroaryl)-1,4-dihydropyridine derivatives.

## 2. Result and discussions

### 2.1. Molecular docking

Modern drug discovery strategies greatly rely on crystallographic 3D structural information of the biomolecular targets. Available X-ray crystallographic data on Protein Data Bank facilitated the performance of virtual structure based drug discovery projects aiming at BACE-1 as a molecular target for Alzheimer disease. In this regard, docking simulation is a key tool in structural molecular biology and computer-assisted drug design (CADD). To explain more, a process to mimic the stereoelectronic fit of ligand and receptor via a lowest energy pathway may be best represented by docking simulations.<sup>27</sup> Numerous successful applications of molecular docking in drug discovery efforts have been reported.<sup>28,29</sup> One of the most popular docking packages is AutoDock. Literature review shows that AutoDock has offered several fruitful advantages in the field of drug design (The AutoDock website: <http://autodock.scripps.edu>).<sup>30</sup>

#### 2.1.1. Docking validation

It is a commonly accepted practice to test a performance of a typical docking protocol via checking its ability in predicting predominant binding mode of a cognate (co-crystallographic) ligand.<sup>31</sup> This procedure is performed via extracting the structure of a cognate ligand and re-docking it into its receptor (self-docking). Success is often interpreted via comparison of root mean square deviation (RMSD) of the Cartesian coordinates of the atoms of the ligand in the docked and crystallographic conformations.

Ten PDB derived BACE-1 structures were subjected to docking validation procedure. PDB structures were chosen on the basis of crystallographic resolutions and also considering relative similarity of co-crystallized ligands to the DHP structures (<http://www.rcsb.org/>). Regarding RMSD values<sup>32</sup> and also conformation

**Table 1**

Docking validation results for different holo PDB structures of BACE-1 using AutoDock4.2

RMSD from reference structure (Å)	Population in the optimum cluster (%)	Maximum no. of energy evaluations	GA runs	Resolution (Å)	PDB code
0.515	47	$5.0 \times 10^6$	100	1.70	2B8L
0.533	80	$5.0 \times 10^6$	100	1.80	2B8V
0.478	88	$5.0 \times 10^6$	100	1.80	2IRZ
0.414	27	$5.0 \times 10^6$	100	2.20	2ISO
1.157	18	$5.0 \times 10^6$	100	1.75	2QMF
0.479	34	$5.0 \times 10^6$	100	1.60	2VJ9
0.845	16	$5.0 \times 10^6$	100	1.80	2QZL
0.756	35	$5.0 \times 10^6$	100	1.79	2VNM
0.486	31	$5.0 \times 10^6$	100	1.80	2P8H
1.616	25	$5.0 \times 10^6$	100	2.05	2VKM

population in the top-ranked cluster of AutoDock output file, we selected 2IRZ as the most appropriate crystallographic structure for further modeling studies. Results of docking validation are summarized in Table 1.

#### 2.1.2. Virtual binding affinities of DHP molecules

The focus of this study was to obtain novel DHP-based BACE-1 inhibitors with the aim of introducing important structural prerequisites for the optimal BACE-1 inhibitory activity. Our initial design strategy was on the basis of developing nonesterified carbamate-based 1,4-DHP derivatives with possibly less calcium channel blocking activity (less side effect)<sup>33</sup> while at the same time mimicking the previously analyzed BACE-1 binding patterns.<sup>34,35</sup> To this end, a pool of 3,5-bis-*N*-(aryl/alkyl) carbamoyl-4-aryl/alkyl-1,4-DHP structures was constructed and subjected to docking simulation (2IRZ; <http://www.rcsb.org/>) Scheme 1.

Docking free energy of binding and the presence of key ligand-residue binding interactions in the BACE-1 active site were considered as screening filters. In the next step, candidate structures were subjected to synthesis followed by enzymatic assessment for their BACE-1 inhibitory activity.

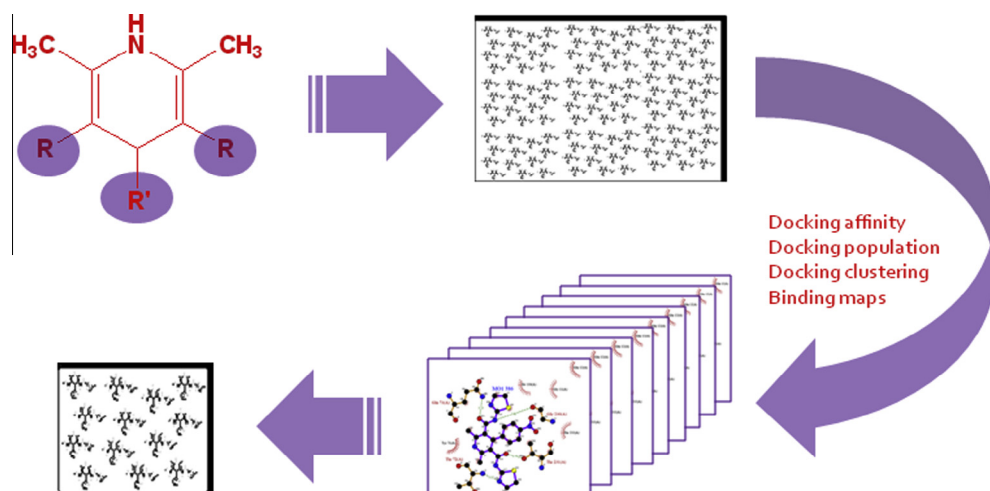
Docking simulations provided some insight into the ligand-receptor interactions. Predicted docking affinities for in vitro hits are summarized in Table 2. To get more information, 2D schematic representation of ligand-receptor interactions for compound **6d** is displayed in Figure 1.

Moreover; ligand-amino acid systems were subjected to optimization process with functional B3LYP in association with triple- $\zeta$  basis set (TZV) to obtain the geometry of H-bonds (Table 3).

## 2.2. Amino acid decomposition analysis

Determination of individual ligand-amino acid binding energies in the active site of the receptor (amino acid decomposition analysis) is a valuable technique in understanding the key interactions between enzyme and inhibitor. Moreover; the process of pharmacophore design might be much more efficient regarding detailed binding energetics of the system. Molecular docking is a popular method for finding probable binding mode and binding affinity of ligand in the active site of the protein with known 3D structure. However, with all advantageous features, docking simulation provides no information on individual ligand-amino acid binding energies in the active site of the biomolecular target. In this regard, ab initio-based amino acid decomposition analysis is a useful approach to the energetics of intermolecular interactions.

According to this rationale and also to compare the effect of ligand structural changes on the contribution of individual residues of BACE-1 active site to the binding energy, we decided to estimate the ligand-residue interaction energies for designed 1,4-DHPs via



**Scheme 1.** Structure based virtual screening of designed DHP library for BACE-1 inhibitory activity

**Table 2**  
Docking simulation results for BACE-1 inhibitors (PDB deposited code: 2LRZ)

Compd. code	$\Delta G_b^a$ (kcal/mol)
<b>6a</b>	-11.31
<b>6b</b>	-11.27
<b>6c</b>	-11.07
<b>6d</b>	-11.14
<b>6e</b>	-11.25
<b>6f</b>	-11.01
<b>6g</b>	-11.23
<b>6h</b>	-11.21
<b>6i</b>	-11.28
<b>6j</b>	-11.01
<b>6k</b>	-11.25
<b>6l</b>	-11.06
<b>6m</b>	-11.03
<b>6n</b>	-11.30
<b>6o</b>	-11.19
<b>6p</b>	-11.33

quantum mechanical methods. To this end, BACE-1 residues sitting within a definite cut off radius from mass center of the ligands (regarding previous crystallographic data; <http://www.rcsb.org/>) were selected as the model system. Our proposed model included DHP molecules and amino acids constructing the active site of BACE-1 (thirty-four residues). Relevant residues were as follows: Gly11, Gln12, Gly13, Tyr14, Leu30, Asp32, Gly34, Ser35, Val69, Pro70, Tyr71, Thr72, Gln73, Phe108, Phe109, Ile110, Trp115, Ile118, Tyr198, Lys224, Ile226, Asp228, Ser229, Gly230, Thr231, Thr232, Asn233, Arg235, Arg307, Ser325, Thr329, Val332, Ala335, and Glu339. All selected amino acids have been previously detected as important residues in binding patterns of various crystallographic BACE-1 inhibitors (<http://www.rcsb.org/>)<sup>3</sup>.

Ligand–residue binding energies ( $\Delta E_b$ ) were calculated by the Eq. 1:

$$\Delta E_b = E_{LR} - E_R - E_L \quad (1)$$

In the above equation,  $E_{LR}$  stands for ligand–residue binding energy, while  $E_R$  and  $E_L$  indicate the electronic energies of unbound residues and ligands, respectively. Various binding energies between 1,4-DHPs and key residues surrounding the active site of BACE-1 were obtained independently at the B3LYP functional in association with triple- $\zeta$  basis set (TZV) level of calculation (summarized in Fig. 2). All ab initio calculations were performed within a fixed number of involved amino acids in order to make

the comparative evaluation possible. It is well understood from the diagram of binding energies (Fig. 2) that nearly similar trends are captured by various designed molecules. This distribution pattern might indicate relatively similar binding poses of 3,5-dicarbamoylated DHPs in the BACE-1 active site.

### 2.3. Conformational analysis

The difference of ligand electronic energies in the optimized and docked conformers may be indicative of conformational instability gain upon binding to the receptor. Accordingly, we decided to model the conformational distortions occurred in the DHP structures as a result of binding to the active site of BACE-1. To this end, compound 6d ( $IC_{50} = 4.21 \mu M$ ) was chosen as a model system for determining the imposed conformational deviation in the BACE-1 active site. In all calculations, dielectric effects of water (i.e. 80) were considered using COSMO model<sup>36</sup>.

Different energies of the evaluated ligand conformations may be a direct outcome of varied internal energies of ligand in its docked and optimized conditions within a biological media ( $\Delta E_{instability}$ ). In this regard,  $\Delta E_{instability}$  is indicative of the torsional instability and should be considered in estimation of binding energies. For calculation of  $\Delta E_{instability}$ , optimized conformation of **6d** was obtained in water and relevant energy was assigned to this unbound conformation.

$\Delta E_{instability}$  may be well related with the free energy of binding via following equations:

$$\Delta G_b = \Delta H_b - T\Delta S \quad (2)$$

$$\Delta H_b = \Delta E_t - P\Delta V \approx \Delta E_{tb} \quad (3)$$

$$\Delta E_{tb} = \Delta E_b + \Delta E_{inst.} \quad (4)$$

Higher  $\Delta E_{instability}$  values provides lower binding energies ( $\Delta E_{tb}$ ) and subsequently weaker ligand–receptor interactions ( $\Delta G_b$ ) would be expected. Conformational instability (kcal/mol) of **6d** upon binding to the BACE-1 active site was found to be 28.59 kcal/mol. The estimated instability value might be indicative of noticeable conformational shifts toward less stable geometric pose. Different geometric poses of **6d** in the docked and minimum energy conformations are shown in Figure 3.

It seemed that functional groups being involved in key interactions with receptor, exhibited sensible torsional distortions and 1,4-DHPs need not necessarily interact with the BACE-1 active site in their optimized conformation. To acquire a quantitative

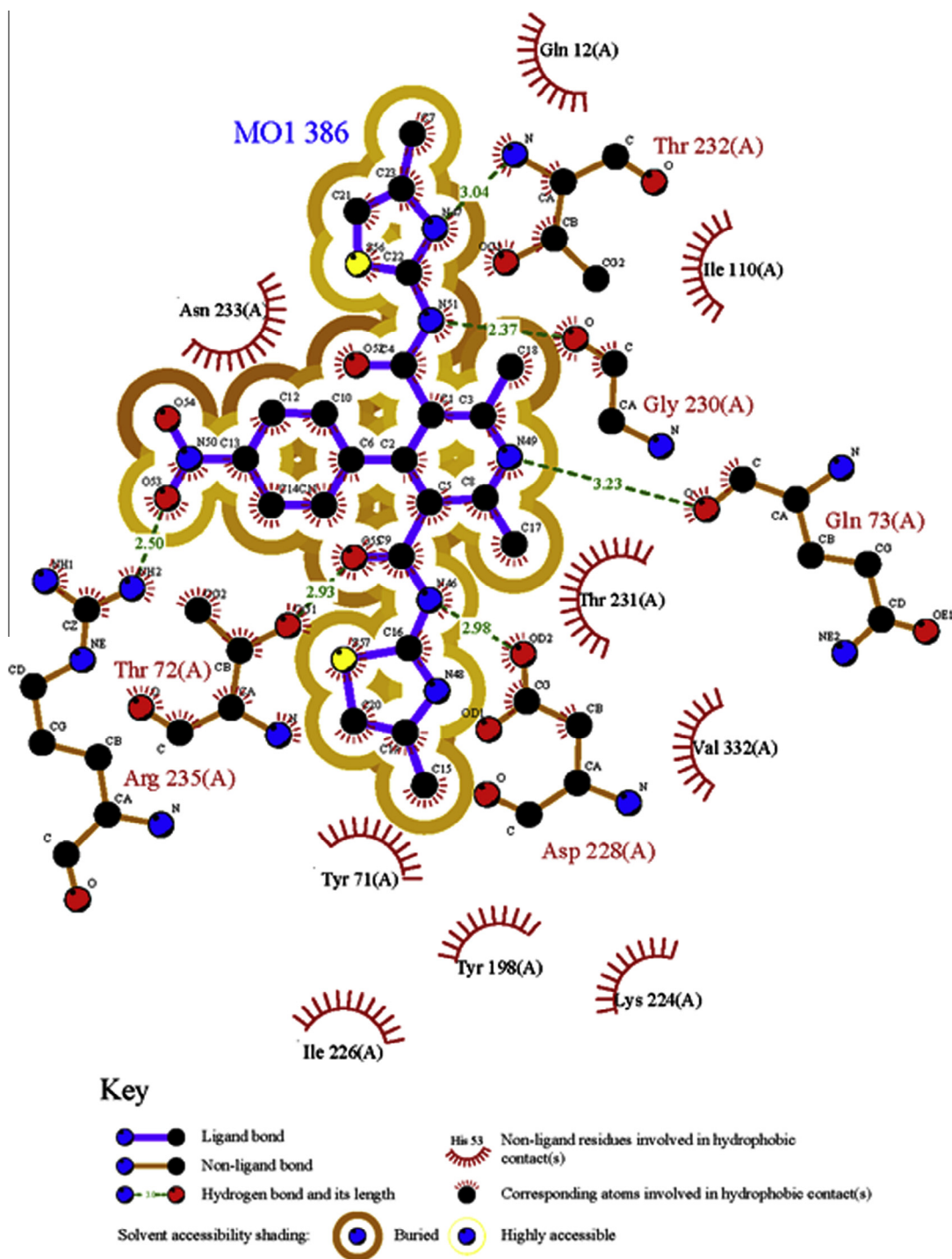


**Figure 1.** 2D scheme of binding interactions between **6d** and BACE-1 active site generated by LIGPLOT, PDB deposition code: 2IRZ.

view on induced conformational changes, estimated geometric parameters (dihedral angles for compound **6d**) are summarized in Table 4.

Our calculations demonstrated that binding of **6d** to the BACE-1 active site was associated with perceptible torsional distortions confirming the obtained instability gain (28.59 kcal/mol). For more elucidation, these changes are highlighted in Table 4. Obtained data demonstrated that C1–C10 and C4–C29 bonds were the molecular sites bearing significant rotations with regard to DHP ring ( $\geq 100^\circ$  distortion) exhibited via altered C2–C1–C10–O11, C2–C1–C10–O12, C2–C4–C29–N30, and C2–C4–C29–N32 dihedral

angles (Table 4). These conformational distortions afforded a proper orientation of amide functionalities to make key H-bonds with Asp228, Gly230 and Thr72 residues of the BACE-1 active site.

Appropriate spatial orientation of thiazole ring in the S2 sub-pocket may be a direct outcome of twisted N12–C14 bond ( $\approx 80^\circ$  distortion). In our interaction maps, the acquired binding pose supported key H-bond with NH of Thr232 backbone (Fig. 3). Similar dihedral shifts could be observed around a N30–C33 bond ( $\approx 96^\circ$  distortion) leading to the lipophilic contacts of another thiazole ring with Lys224 ( $-0.76$  kcal/mol) and Tyr198 ( $-1.22$  kcal/mol) residues of the BACE-1 active site.

**Table 3**  
Estimated hydrogen bond distances (Å) for docked DHP BACE-1 inhibitors

Compd. code	Participant amino acids <sup>a</sup>	Optimized hydrogen bond distances (Å)	Involved atom of the ligand	Involved atom of the amino acid
<b>6a</b>	Thr72	2.36	(Amide) O	(Side chain) OH
	Gln73	2.49	(DHP) NH	(Backbone) C=O
	Asp228	2.38	(Amide) NH	(Side chain) COO <sup>-</sup>
	Gly230	2.02	(Amide) NH	(Backbone) C=O
	Thr231	2.57	(Furyl) O	(Side chain) OH
	Thr232	2.27	(Thiazole) N	(Backbone) NH
<b>6b</b>	Thr72	2.45	(Amide) O	(Side chain) OH
	Gln73	2.63	(DHP) NH	(Backbone) C=O
	Asp228	2.51	(Amide) NH	(Side chain) COO <sup>-</sup>
	Gly230	2.09	(Amide) NH	(Backbone) C=O
	Thr232	2.29	(Thiazole) N	(Backbone) OH
	Arg235	2.23	(Nitro) O	(Side chain) NH <sub>2</sub>
<b>6c</b>	Thr72	2.01	(Amide) O	(Side chain) OH
	Gln73	2.58	(DHP) NH	(Backbone) C=O
	Asp228	2.06	(Amide) NH	(Side chain) COO <sup>-</sup>
	Gly230	2.13	(Amide) NH	(Backbone) C=O
	Arg235	2.17	(Nitro) O	(Side chain) NH <sub>2</sub> <sup>+</sup>
<b>6d</b>	Thr72	2.50	(Amide) O	(Side chain) OH
	Gln73	2.34	(DHP) NH	(Backbone) C=O
	Asp228	2.30	(Amide) NH	(Side chain) COO <sup>-</sup>
	Gly230	2.02	(Amide) NH	(Backbone) C=O
	Thr232	2.43	(Thiazole) N	(Backbone) NH
	Arg235	2.18	(Nitro) O	(Side chain) NH <sub>2</sub> <sup>+</sup>
<b>6e</b>	Thr72	2.44	(Amide) O	(Side chain) OH
	Gln73	2.59	(DHP) NH	(Backbone) C=O
	Asp228	2.46	(Amide) NH	(Side chain) COO <sup>-</sup>
	Gly230	2.05	(Amide) NH	(Backbone) C=O
	Thr232	2.34	(Benzothiazole) N	(Backbone) NH
	Arg235	2.08	(Nitro) O	(Side chain) NH <sub>2</sub> <sup>+</sup>
<b>6f</b>	Thr72	2.16	(Amide) O	(Side chain) OH
	Gln73	2.49	(DHP) NH	(Backbone) C=O
	Asp228	2.05	(Amide) NH	(Side chain) COO <sup>-</sup>
	Gly230	2.14	(Amide) NH	(Backbone) C=O
	Asn233	2.46	(Nitro) O	(Backbone) NH
<b>6g</b>	Thr72	2.15	(Amide) O	(Side chain) OH
	Gln73	2.50	(DHP) NH	(Backbone) C=O
	Asp228	2.38	(Amide) NH	(Side chain) COO <sup>-</sup>
	Gly230	2.17	(Amide) NH	(Backbone) C=O
	Thr232	2.54	(Thiazole) N	(Backbone) NH
	Asn233	2.31	(Nitro) O	(Backbone) NH
<b>6h</b>	Thr72	2.36	(Amide) O	(Side chain) OH
	Gln73	2.54	(DHP) NH	(Backbone) C=O
	Asp228	2.36	(Amide) NH	(Side chain) COO <sup>-</sup>
	Gly230	2.00	(Amide) NH	(Backbone) C=O
	Thr232	2.33	(Benzothiazole) O	(Backbone) NH
	Asn233	2.32	(Nitro) O	(Backbone) NH
<b>6i</b>	Thr72	2.31	(Amide) O	(Side chain) OH
	Gln73	2.42	(DHP) NH	(Backbone) C=O
	Asp228	2.43	(Amide) NH	(Side chain) COO <sup>-</sup>
	Gly230	1.89	(Amide) NH	(Backbone) C=O
	Thr232	2.70	(benzothiazole) N	(Backbone) NH
	Asn233	2.79	(Nitro) O	(Backbone) NH
<b>6j</b>	Arg307	2.19	(Ethoxy) O	(Side chain) NH <sub>2</sub> <sup>+</sup>
	Thr72	2.21	(Amide) O	(Side chain) OH
	Gln73	2.61	(DHP) NH	(Backbone) C=O
	Asp228	2.13	(Amide) NH	(Side chain) COO <sup>-</sup>
	Gly230	2.04	(Amide) NH	(Backbone) C=O
<b>6k</b>	Asn233	2.52	(Nitro) O	(Backbone) NH
	Thr72	2.29	(Amide) O	(Side chain) OH
	Gln73	2.65	(DHP) NH	(Backbone) C=O
	Asp228	2.43	(Amide) NH	(Side chain) COO <sup>-</sup>
	Gly230	2.11	(Amide) NH	(Backbone) C=O
	Thr232	2.21	(Benzothiazole) N	(Backbone) NH
<b>6l</b>	Asn233	2.30	(Nitro) O	(Backbone) NH
	Thr72	2.56	(Amide) O	(Side chain) OH
	Gln73	2.37	(DHP) NH	(Backbone) C=O
	Asp228	2.25	(Amide) NH	(Side chain) COO <sup>-</sup>
	Gly230	2.19	(Amide) NH	(Backbone) C=O
<b>6m</b>	Thr231	2.79	(Pyrrole) NH	(Side chain) OH
	Thr72	2.19	(Amide) O	(Side chain) OH
	Gln73	2.50	(DHP) NH	(Backbone) C=O
	Asp228	2.44	(Amide) NH	(Side chain) COO <sup>-</sup>
	Gly230	2.16	(Amide) NH	(Backbone) C=O
	Thr232	2.25	(Benzothiazole) N	(Backbone) NH

(continued on next page)

Table 3 (continued)

Compd. code	Participant amino acids <sup>a</sup>	Optimized hydrogen bond distances (Å)	Involved atom of the ligand	Involved atom of the amino acid
<b>6n</b>	Thr72	1.99	(Amide) O	(Side chain) OH
	Gln73	2.68	(DHP) NH	(Backbone) C=O
	Asp228	2.71	(Amide) NH	(Side chain) COO <sup>-</sup>
	Gly230	2.17	(Amide) NH	(Backbone) C=O
	Thr232	2.84	(Benzothiazole) N	(Backbone) NH
<b>6o</b>	Thr72	2.29	(Amide) O	(Side chain) OH
	Gln73	2.46	(DHP) NH	(Backbone) C=O
	Asp228	2.32	(Amide) NH	(Side chain) COO <sup>-</sup>
	Gly230	2.06	(Amide) NH	(Backbone) C=O
	Thr232	2.45	(Thiazole) N	(Backbone) NH
	Arg235	2.53	(Methoxy) O	(Side chain) NH <sub>2</sub> <sup>+</sup>

<sup>a</sup> H-bond distances have been reported as (H...acceptor) lengths.

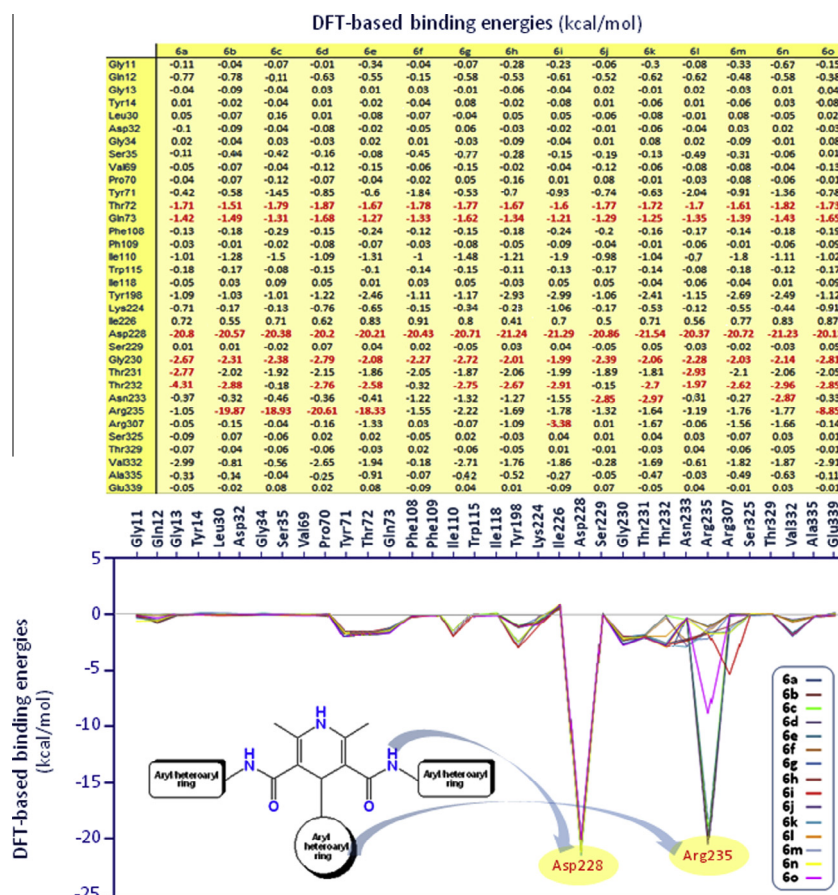


**Figure 2.** DFT-based binding energies of 3,5-dicarbamoylated DHPs into the BACE-1 active site residues, binding energies attributed to H-bonds are bold-highlighted in the upper table. In the lower chart, most favored binding energies are addressed toward their site of interactions.

Other noticeable rotations occurred around a C2–C20 ( $\approx 30^\circ$ ) and C23–N26 ( $\approx 50^\circ$ ) bonds leading to the disturbed co-planarity of nitro substituent with the phenyl ring and appropriate H-bond interaction with guanidinium side chain of Arg235. The results of this study may be best explained by this statement that ligands tolerated some bond torsions to achieve key binding features in the receptor active site leading to the stabilization of ligand–receptor complex.

#### 2.4. Chemistry

In an attempt to provide the structural features for BACE-1 inhibitory activity, a series of DHP derivatives were synthesized (**6a–p**, Table 7). Synthesis of desired 2,6-dimethyl-4-aryl/heteroaryl-

3,5-bis-*N*-(aryl/heteroaryl) carbamoyl-1,4-dihydropyridines (**6a–p**) was achieved via molecular condensation of corresponding aldehydes (**4**), appropriate *N*-aryl-acetoacetamide derivatives (**3a–e**) and ammonium acetate (**5**) in absolute ethanol (Scheme 2).

Our results showed that corresponding DHPs were obtained in good yields and shorter reaction times using nano-Fe<sub>3</sub>O<sub>4</sub> catalyst in EtOH (Table 7). Several other results for nano-catalyzed synthesis of DHPs also indicated a higher synthetic yields and shorter reaction times in ethanol.<sup>37,38</sup> An efficient synthesis of some esterified 1,4-DHP scaffolds by nano-Fe<sub>3</sub>O<sub>4</sub> particles was previously reported in the literature.<sup>39</sup>

On the basis of general knowledge, following mechanistic hypothesis may be proposed for nano-catalyzed cyclocondensation reaction (Scheme 3).<sup>38</sup> It is believed that nano-Fe<sub>3</sub>O<sub>4</sub> particles

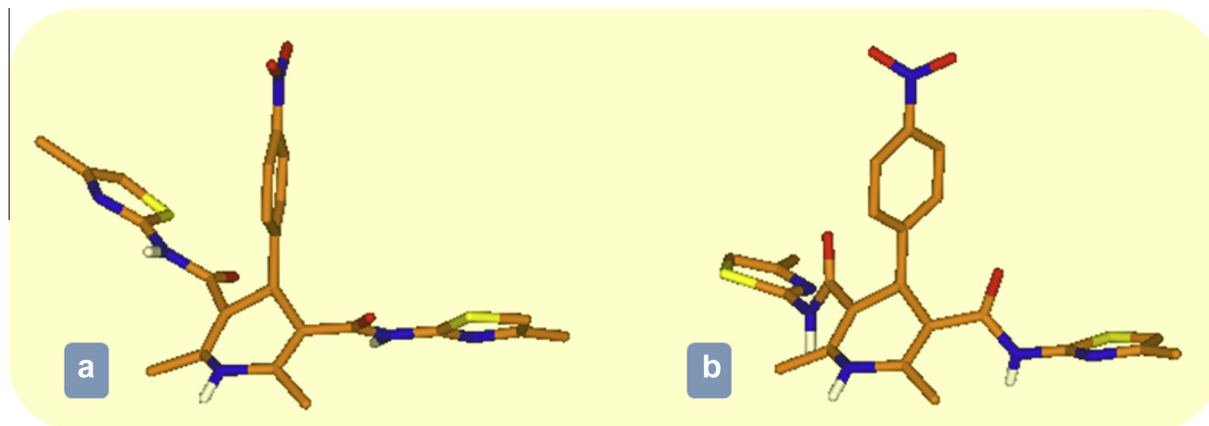


**Figure 3.** Conformation of **6d** in (a) DFT-optimized and (b) docked pose (BACE-1 active site).

possess efficient Lewis acid sites incorporating higher electrophilicity into *N*-arylacetoacetamides and enabling facile approaching of ammonia and enamines.

## 2.5. Biological assessments

### 2.5.1. BACE-1 inhibitory activity and structure activity relationship (SAR)

BACE-1 inhibitory activities of synthesized 1,4-DHPs were determined using a fluorescence resonance energy transfer (FRET) based BACE-1 kit that included BACE-1 enzyme and specific APP-based peptide substrate (Rh-EVNLDAEFK-quencher). IC<sub>50</sub> values were determined for compounds exhibiting minimum 50% BACE-1 inhibitory activity at 10 μM. Experiments were repeated for three to four times for each compound under study. Results are summarized in Table 5.

A relatively reliable correlation could be obtained between docking affinities and in vitro BACE-1 inhibitory activities in terms of log<sub>10</sub> (I<sub>10</sub>: BACE-1 inhibition% at 10 μM) (Fig. 4).

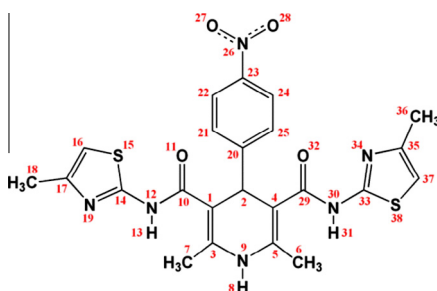
Generally, the active site of BACE-1 is composed of 8 sub-pockets that are designated as S1, S2, S3, S4, S'1, S'2, S'3 and S'4. These subsites are the correspondent binding pockets of BACE-1 active site for the peptidic inhibitors (P1, P2, P3, P4, P'1, P'2, P'3 and P'4).<sup>40</sup> SAR analysis of DHP molecules in accordance with molecular modeling results indicated that designed DHP molecules made H-bonds and hydrophobic contacts with some of these sub-pockets. For more information on sub-pockets, readers may be referred to the previous publication.<sup>34</sup> Regarding this, following points may be concluded:

- (1) Among studied molecules, achieving a desirable BACE-1 inhibitory activity might be possible through electrostatic interactions including H-bonds. All the 3,5-dicarbamoylated DHP hits participated in key H-bond interactions with Asp228 (supported by favorable binding energies; Fig. 2) and Gly230 sitting in the region between S1 and S2 subsites. In this regard, diagram of DFT-based binding energies (Fig. 2) might be characterized by two distinguishing minima that were related to the charge-assisted H-bonds of DHP molecules with Asp228 and Arg235 residues of the BACE-1 active site (Fig. 5).
- (2) The most potent compound (**6d**) had an IC<sub>50</sub> value of 4.21 μM. Docking/ab initio studies revealed that compound **6d** might participate in key H-bonds with Arg235, Thr232, Thr72, Asp228, and Gly230 in the S1 and S2 subsites. Detailed analysis of hydrophobic binding patterns showed that these contacts might be envisaged between Val332

and sulfur atom of thiazole/benzothiazole rings in DHPs. Moreover; methyl substituent of the thiazole ring might be responsible for further hydrophobic interactions with Lys224 in the S'2 subpocket. It should be noted that these hydrophobic contacts might be weaker for 6b-Lys224 and 6b-Val332 interactions (Fig. 2). Similar reports can be found in the literature.<sup>41</sup>

- (3) As it could be clearly understood from the data in Table 5 and 4-nitrophenyl and 2-nitrophenyl aromatic groups on the C4 position of DHP ring might be better tolerated without significant loss of activity when compared to 3-nitrophenyl substituent (**6d**; IC<sub>50</sub> = 4.21 μM; **6k**; IC<sub>50</sub> = 4.27 μM). Our theoretical studies showed that this priority might be attributed to efficient H-bonds with Arg235 and Asn233 in 4-nitrophenyl and 2-nitrophenyl-substituted series, respectively. However the introduction of polar heteroaryl rings to the C4 position of DHP ring maintained the binding affinity (**6a** and **6l**). Compound **6l** (containing 2-pyrrole ring) was the most potent compound in the 3,5-bis-*N*-(5-methylisoxazol-3-yl) carbamoyl substituted series. Similar trend could be observed for compound **6a** which possessed IC<sub>50</sub> value of 6.78 μM (Table 5).
- (4) Contribution of H-bonds to the binding affinity of more polar DHP molecules (**6c**, **6f**, **6i**, **6j**, and **6l**) might be greatly depended on solvation/desolvation effects. This could be apparently detected considering lower binding affinity of **6i** when compared to **6h** and **6k** (despite close docking affinities, Table 2). Indeed, larger polarities may be paid for by higher desolvation penalties.
- (5) 3,5-Bis-*N*-(5-methyl-3-isoxazolyl) carbamoylated DHPs (**6c**, **6f**, **6j** and **6l**) had lower BACE-1 inhibitory activities (Table 5). For these derivatives, modeling studies showed no sign of key H-bond(s) to Thr232. This might be attributed to the geometric orientation of isoxazole ring in the active site of BACE-1. Compounds **6a**, **6b**, **6d**, **6e**, **6g**, **6h**, **6i**, **6k**, **6m**, **6n** and **6o** interacted with S2 subpocket through H-bonds between Thr232 backbone NH and thiazole/benzothiazole nitrogen atom.
- (6) A charge-assisted H-bond interaction with Arg235 guanidinium group might be envisaged through H-acceptor moieties (–NO<sub>2</sub>) of the para position of C4-substituted aryl ring. It should be noted that **6o** interacted with Arg235 via its *para*-methoxy substituent. While compared to **6b**, **6c**, **6d** and **6e**, this interaction was supported by lower binding energy (–8.85 kcal/mol). Moreover, binding poses indicated that aromatic ring of DHPs stacked near to the guanidinium group so that its π electrons might tend to stabilize a partial

**Table 4**  
Dihedral angles of **6d** in the DFT-optimized and docked conformers (BACE-1 active site)



Dihedral angle	Angle (degree)		Dihedral angle	Angle (degree)	
	docked pose	Optimized pose		docked pose	Optimized pose
C(3)–C(1)–C(2)–C(4)	8.480	8.435	H(13)–N(12)–C(14)–S(15)	94.890	175.968
C(3)–C(1)–C(2)–C(20)	–116.802	–116.795	H(13)–N(12)–C(14)–N(19)	–85.402	–4.372
C(10)–C(1)–C(2)–C(4)	–167.550	–167.562	N(12)–C(14)–S(15)–C(16)	179.717	179.687
C(10)–C(1)–C(2)–C(20)	67.240	67.208	N(19)–C(14)–S(15)–C(16)	–0.013	0.001
C(2)–C(1)–C(3)–C(7)	–179.212	–179.183	N(12)–C(14)–N(19)–C(17)	–179.819	–179.785
C(2)–C(1)–C(3)–N(9)	0.730	0.677	S(15)–C(16)–N(19)–C(17)	–0.086	–0.096
C(10)–C(1)–C(3)–C(7)	–3.599	–3.529	C(14)–S(15)–C(16)–C(17)	0.109	0.095
C(10)–C(1)–C(3)–N(9)	176.342	176.133	S(15)–C(16)–C(17)–C(18)	179.774	179.739
C(2)–C(1)–C(10)–O(11)	–50.182	56.622	S(15)–C(16)–C(17)–N(19)	–0.186	–0.174
C(2)–C(1)–C(10)–N(12)	131.126	–126.098	C(16)–C(17)–N(19)–C(14)	0.172	0.171
C(3)–C(1)–C(10)–O(11)	133.860	–123.375	C(18)–C(17)–N(19)–C(14)	–179.879	–179.746
C(3)–C(1)–C(10)–N(12)	–44.832	57.905	C(2)–C(20)–C(21)–C(22)	–179.810	–179.840
C(1)–C(2)–C(4)–C(5)	–9.530	–9.503	C(25)–C(20)–C(21)–C(22)	0.417	0.448
C(1)–C(2)–C(4)–C(29)	172.017	172.07	C(2)–C(20)–C(25)–C(24)	179.811	179.818
C(20)–C(2)–C(4)–C(5)	114.770	114.804	C(21)–C(20)–C(25)–C(24)	–0.410	–0.461
C(20)–C(2)–C(4)–C(29)	–63.682	–63.675	C(20)–C(21)–C(22)–C(23)	0.017	–0.024
C(1)–C(2)–C(20)–C(21)	99.915	97.451	C(21)–C(22)–C(23)–C(24)	–0.468	–0.394
C(1)–C(2)–C(20)–C(25)	–113.311	–82.835	C(21)–C(22)–C(23)–N(26)	179.818	179.819
C(4)–C(2)–C(20)–C(21)	–57.957	–27.444	C(22)–C(23)–C(24)–C(25)	0.475	0.381
C(4)–C(2)–C(20)–C(25)	121.818	152.270	N(26)–C(23)–C(24)–C(25)	–179.810	–179.833
C(1)–C(3)–N(9)–C(5)	–9.970	–9.940	C(22)–C(23)–N(26)–O(27)	–52.516	–1.577
C(1)–C(3)–N(9)–H(8)	–175.136	–175.040	C(22)–C(23)–N(26)–O(28)	127.433	178.501
C(7)–C(3)–N(9)–C(5)	169.975	169.927	C(24)–C(23)–N(26)–O(27)	127.766	178.633
C(7)–C(3)–N(9)–H(8)	4.809	4.827	C(24)–C(23)–N(26)–O(28)	–52.285	–1.288
C(2)–C(4)–C(5)–C(6)	–179.524	–17.539	C(23)–C(24)–C(25)–C(20)	–0.033	0.051
C(2)–C(4)–C(5)–N(9)	1.535	1.482	C(4)–C(29)–N(30)–C(33)	177.486	177.491
C(29)–C(4)–C(5)–C(6)	–1.133	–1.119	C(4)–C(29)–N(30)–H(31)	0.857	0.791
C(29)–C(4)–C(5)–N(9)	179.926	179.902	O(32)–C(29)–N(30)–C(33)	–3.050	–3.034
C(2)–C(4)–C(29)–N(30)	–125.518	–62.974	O(32)–C(29)–N(30)–H(31)	–179.679	–179.734
C(2)–C(4)–C(29)–O(32)	55.029	117.562	C(29)–N(30)–C(33)–N(34)	84.511	–178.765
C(5)–C(4)–C(29)–N(30)	55.955	118.513	C(29)–N(30)–C(33)–S(38)	–95.175	1.528
C(5)–C(4)–C(29)–O(32)	–123.458	–60.951	H(31)–N(30)–C(33)–N(34)	–98.803	–2.014
C(4)–C(5)–N(9)–C(3)	8.853	8.876	H(31)–N(30)–C(33)–S(38)	81.510	178.279
C(4)–C(5)–N(9)–H(8)	174.048	174.009	N(30)–C(33)–N(34)–C(35)	–179.743	–179.782
C(6)–C(5)–N(9)–C(3)	–170.152	–170.65	S(38)–C(33)–N(34)–C(35)	–0.030	–0.050
C(6)–C(5)–N(9)–H(8)	–4.958	–5.032	C(30)–C(33)–C(38)–H(37)	179.692	179.732
C(1)–C(10)–N(12)–C(14)	179.054	179.021	N(34)–C(33)–C(38)–C(37)	–0.018	0.002
C(1)–C(10)–N(12)–H(13)	3.119	3.051	C(33)–N(34)–C(35)–C(36)	0.078	–179.898
O(11)–C(10)–N(12)–C(14)	0.350	0.289	C(33)–N(34)–C(35)–C(37)	–179.856	0.087
O(11)–C(10)–N(12)–H(13)	–175.586	–175.682	N(34)–C(35)–C(37)–S(38)	–0.093	–0.088
C(10)–N(12)–C(14)–S(15)	–81.093	–0.047	C(36)–C(35)–C(37)–S(38)	179.839	179.897
C(10)–N(12)–C(14)–N(19)	98.614	179.613	C(35)–C(37)–S(38)–C(33)	0.061	0.047

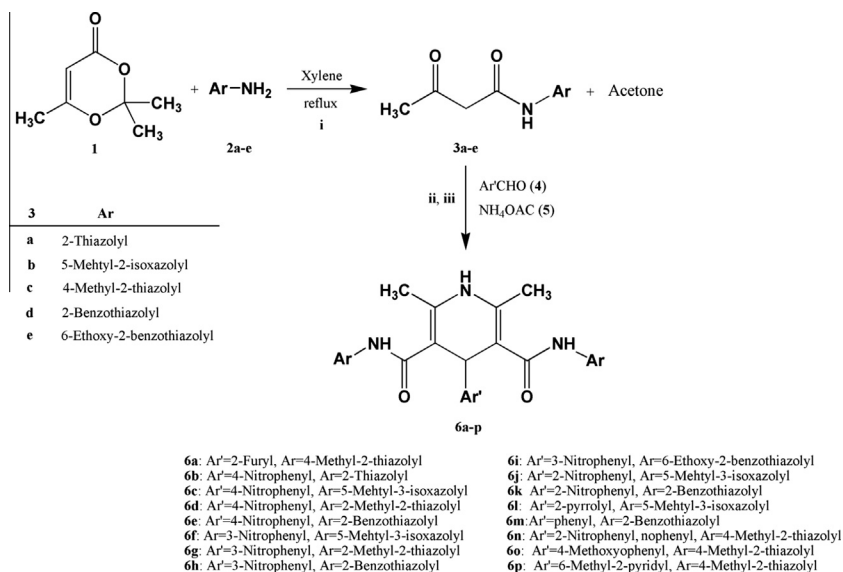
positive charge on the NH of guanidinium group providing a possible  $\pi$ -cation interaction. Binding pose studies and interaction energies (Fig. 2) indicated that in the case of Asn233, these interactions were nonbonded contacts (van der Waals) (except for **6j** and **6k** that contributed to H-bonds with Asn233).

(7) All of the docked DHP structures represented a boat like conformation in the active site of the BACE-1. This boat like conformation of DHP ring in the active site of the BACE-1 might take part in key H-bond with carbonyl oxygen of Gln73 backbone (Fig. 6).

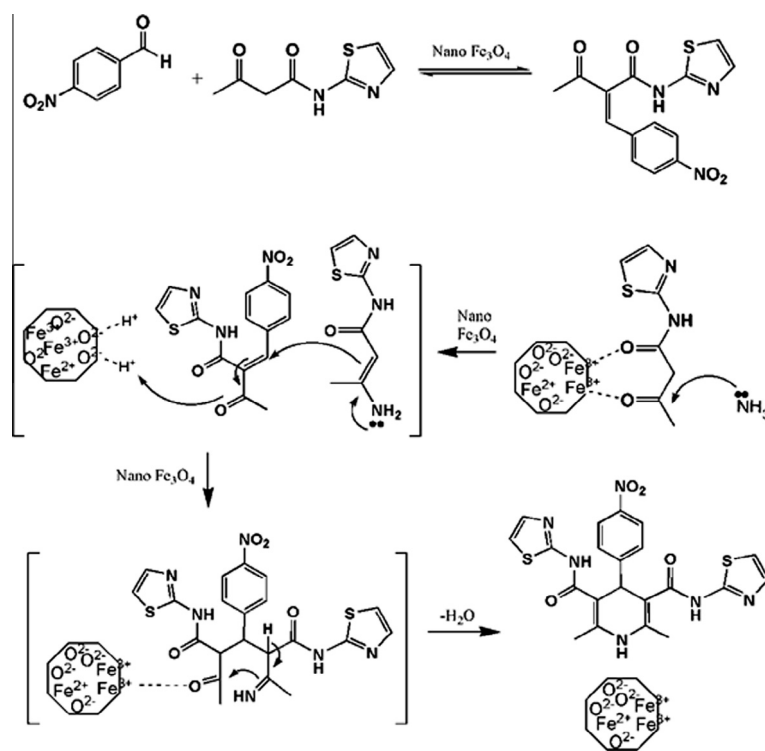
(8) In the C4 position of the DHP ring, incorporation of five-member heterocycles (furan and pyrrole) instead of phenyl rings might be well tolerated without significant loss of BACE-1 inhibitory activity (**6a**; 66.38% inhibition and **6d**; 77.22% inhibition at 10  $\mu$ M).

(9) Tyr71 (flap residue) contributed to hydrophobic contacts with C2 and/or C6 methyl groups of all DHP rings via its side chain benzyl site. These interactions were associated with binding energies in the range of –1.52 to –1.98 kcal/mol.

(10) Ligand–residue binding energies and docked poses indicated that compounds **6e**, **6h**, **6i**, **6k**, and **6m** might participate in



**Scheme 2.** Synthesis of compounds (**6a–p**). Reagents and conditions: (i) xylene, reflux, 2–4 h, (ii) EtOH, reflux, 24–48 h, (iii) EtOH, 20 mol% nano-Fe<sub>3</sub>O<sub>4</sub>, 1–10 h.



**Scheme 3.** Possible mechanistic view of nano-Fe<sub>3</sub>O<sub>4</sub> catalyzed cyclocondensation of ammonia, *N*-arylacetoacetamides and aldehydes leading to DHP molecules.

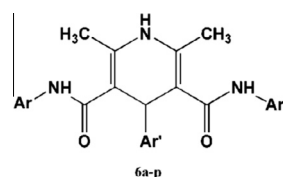
favorable  $\pi$ – $\pi$  stacking contacts with Tyr198 via their fused aromatic rings (supported by  $-2.41$  to  $-2.99$  kcal/mol). Nearly parallel orientation of aromatic rings (Tyr198 phenyl ring and ligand benzothiazole ring) might be responsible for detected  $\pi$ – $\pi$  stacking interaction (Fig. 7).

- (11) Arg307 made weak to moderate lipophilic contacts with benzothiazole containing structures. Extended well oriented structure of **6i** (C6'-ethoxy group) provided additional H-bond interaction with Arg307 (NH-2 of guanidine side chain, Fig. 7) in the S4 subpocket.

### 2.5.2. Calcium channel blocking activity

In the present work, developed compounds had essential requirement for calcium channel blocking activity as belonging to the DHP class. Due to this rationale, superior BACE-1 inhibitors (**6a**, **6d**, **6k** and **6n**) were evaluated as calcium channel antagonists using high potassium ion concentration in guinea-pig ileal longitudinal smooth muscle. The calcium channel blocking activities were determined as the concentration needed to produce 50% inhibition of the guinea-pig ileal longitudinal smooth muscle contractility (Summarized in Table 6).

**Table 5**  
In vitro BACE-1 inhibitory activities of compounds **6a–p**



Compd.	Ar	Ar'	Inhibition at 50 $\mu\text{M}^a$ (%)	Inhibition at 10 $\mu\text{M}$ (%)	$\text{IC}_{50}^b$ ( $\mu\text{mol/L}$ )
<b>6a</b>	4-Methyl-2-thiazolyl	2-Furyl	95.12 $\pm$ 4.29	66.38 $\pm$ 5.15	6.78 $\pm$ 0.54
<b>6b</b>	2-Thiazolyl	4-Nitrophenyl	46.76 $\pm$ 6.69	28.14 $\pm$ 6.03	—
<b>6c</b>	5-Methyl-3-isoxazolyl	4-Nitrophenyl	42.98 $\pm$ 11.56	23.50 $\pm$ 5.18	—
<b>6d</b>	4-Methyl-2-thiazolyl	4-Nitrophenyl	88.01 $\pm$ 3.97	77.22 $\pm$ 3.64	4.21 $\pm$ 0.11
<b>6e</b>	2-Benzothiazolyl	4-Nitrophenyl	90.83 $\pm$ 6.59	49.84 $\pm$ 2.99	—
<b>6f</b>	5-Methyl-3-isoxazolyl	3-Nitrophenyl	ND <sup>c</sup>	11.63 $\pm$ 3.34	—
<b>6g</b>	4-Methyl-2-thiazolyl	3-Nitrophenyl	70.37 $\pm$ 6.26	34.76 $\pm$ 6.32	—
<b>6h</b>	2-Benzothiazolyl	3-Nitrophenyl	56.16 $\pm$ 3.05	49.35 $\pm$ 2.23	—
<b>6i</b>	6-Ethoxy-2-benzothiazolyl	3-Nitrophenyl	93.97 $\pm$ 4.63	49.06 $\pm$ 5.02	—
<b>6j</b>	5-Methyl-3-isoxazolyl	2-Nitrophenyl	53.96 $\pm$ 11.13	12.72 $\pm$ 1.54	—
<b>6k</b>	2-Benzothiazolyl	2-Nitrophenyl	87.15 $\pm$ 2.22	65.56 $\pm$ 4.29	4.27 $\pm$ 0.65
<b>6l</b>	5-Methyl-3-isoxazolyl	2-Pyrrolyl	57.39 $\pm$ 1.33	24.13 $\pm$ 8.31	—
<b>6m</b>	2-Benzothiazolyl	Phenyl	ND	44.93 $\pm$ 2.20	—
<b>6n</b>	4-Methyl-2-thiazolyl	2-Nitrophenyl	94.95 $\pm$ 3.70	69.38 $\pm$ 7.59	4.66 $\pm$ 2.24
<b>6o</b>	4-Methyl-2-thiazolyl	4-Methoxyphenyl	86.35 $\pm$ 7.92	44.42 $\pm$ 10.71	—
<b>6p</b>	4-Methyl-2-thiazolyl	6-Methyl-2-pyridyl	ND	ND	—
OM99-2 <sup>d</sup>	—	—	—	—	0.003( $\pm$ 0.00)

<sup>a</sup> Values represent means  $\pm$  standard error (S.E.) of three to five independent experiments.

<sup>b</sup>  $\text{IC}_{50}$  values determined for compounds achieving over % 50 BACE-1 inhibition at 10  $\mu\text{M}$ .

<sup>c</sup> There was an interference of compound with fluorescence resonance energy transfer (FRET) assay.

<sup>d</sup> OM99 was tested at 10, 1 and 0.1 nM.

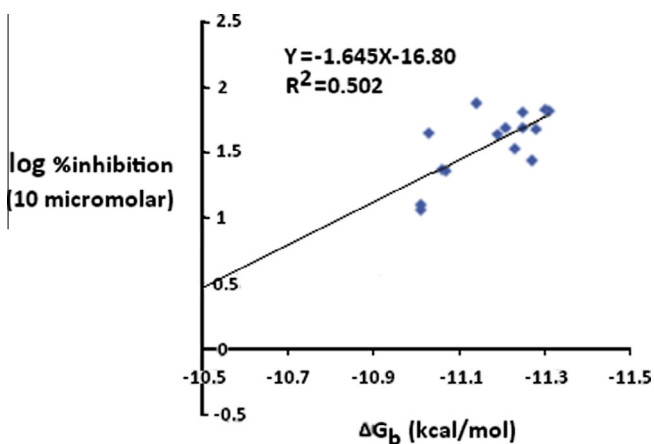


**Figure 4.** Correlation of docking binding energies with BACE-1 inhibitory activities).

According to the obtained data, all of the assessed compounds exhibited low calcium channel blocking activity ( $\text{IC}_{30} = 3.48 \times 10^{-6}$  to  $2.66 \times 10^{-5}$ ) when compared to nifedipine ( $\text{IC}_{30} = 9.27 \times 10^{-9}$ ).

### 3. Conclusion

Small molecule BACE-1 inhibitors could be successfully developed as in vitro hits via structure-based virtual screening of a library of 3,5-bis-*N*-(aryl) carbamoylated DHPs. Ab initio calculations of interaction energies were complementary to the molecular docking simulations in modeling of DHP-based BACE-1 inhibitors. The most potent compound (**6d**) had an  $\text{IC}_{50}$  of 4.21  $\mu\text{M}$  in the FRET assay. Molecular modeling studies showed that well-oriented H-bond donors/acceptors might play a central

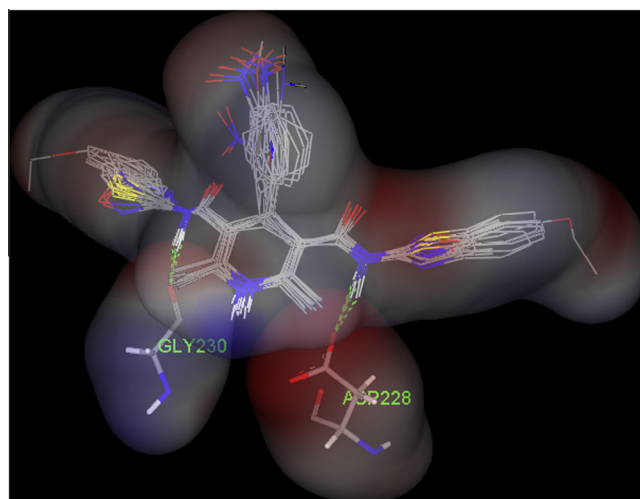


**Figure 5.** Superimposed docked poses of DHP molecules in the active site of BACE-1.

role in BACE-1 inhibitory activity of 3,5-bis-*N*-(aryl) carbamoylated DHPs. Results demonstrated that the solvation/desolvation effects should be considered in interpretation of binding affinity results of more polar DHP derivatives. SAR exploration of developed BACE-1 inhibitors demonstrated the vital role of two carbamoyl NHs of 3,5-disubstituted aryl/heteroaryl-carbamoyl-1,4-DHPs in making key H-bonds with Asp228 and Gly230. Residing in the same plane with Asp228, the amide groups of DHP molecules contributed to monodentate H-bonds with aspartate oxygens of Asp228 (H-bond distance range = 2.05–2.71 Å) and backbone carbonyl oxygen of Gly230 (H-bond distance range = 1.89–2.19 Å). In confirmation of previous results, our biological data suggested that although much favoured, the direct H-bonding interactions

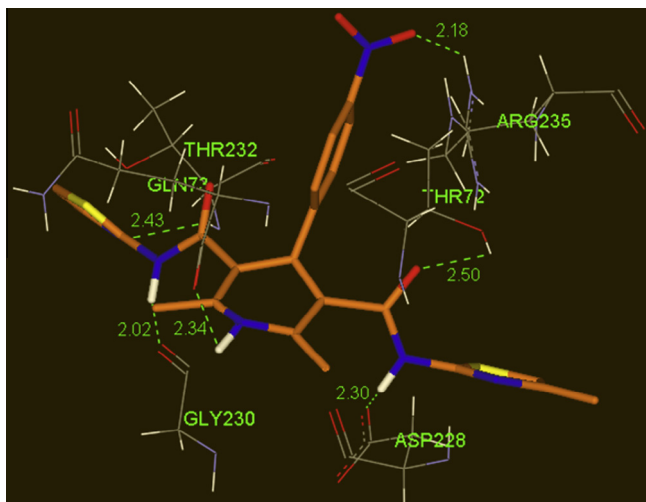


**Figure 6.** Possible H-binding pattern of docked DHP (**6d**) in the BACE-1 active site.

between the ligand and two components of Asp dyad might not be necessarily important for BACE-1 inhibition and an adaptable level of inhibition might be expected through H-bond with Asp228.<sup>15</sup> 3,5-Bis-*N*-4-methyl-2-thiazolyl and 3,5-bis-*N*-2-benzothiazolyl substituted DHP structures (bearing well oriented H-acceptors on their C4-substituted aromatic rings) are ideal cases for further extension to S4, S3, S1 and S2 subpockets with the aim of achieving more potent small molecule BACE-1 inhibitors. Moreover, further biological assessment of the DHP compounds (**6a**, **6d**, **6k** and **6n**) revealed significantly lower calcium channel blocking activity with regard to nifedipine. Therefore the offered DHP structures might be judged as potential BACE-1 inhibitors without possible side effect(s). Further work will focus on more extended decorations within N<sup>3</sup>- and N<sup>5</sup>-substituents of DHP molecules in the symmetric/nonsymmetric framework.

## 4. Materials and methods

### 4.1. Computational section

#### 4.1.1. Molecular docking study

Flexible-ligand docking studies were carried out using AutoDock version 4.2.<sup>42</sup> All the X-ray crystallographic holo structures of BACE-1 were retrieved from the Brookhaven protein data bank

(<http://www.rcsb.org/>). The protein structure was subjected to optimization step in order to minimize the crystallographic induced bond clashes using steepest descent method by Gromacs package.<sup>43</sup> For preparation of a target protein as a template (PDB code: 2IRZ), cognate ligand (IO2) and all crystallographic water molecules were removed from the original receptor structure. All the pre-processing steps for receptor crystallographic structure were performed via WHAT IF server (<http://swift.cmbi.ru.nl/servers/html/prepdock.html/>) European Molecular Laboratory Heidelberg, Germany) and AutoDock Tools 1.5.4 program (ADT).<sup>42</sup> ADT program was used to merge nonpolar hydrogens into related carbon atoms of the receptor and Kollman charges were also assigned. For docked ligands, nonpolar hydrogens were added; Gasteiger charges assigned and torsions degrees of freedom were also allocated by ADT program. Lamarckian genetic algorithm (LGA) was applied to model the interaction/binding between DHPs and BACE-1 active site. Desirable independent genetic algorithm (GA) runs were considered for each ligand under study. For Lamarckian GA; 27,000 maximum generations; a gene mutation rate of 0.02; and a crossover rate of 0.8 were used.

The grid maps characterizing the protein in the actual docking procedure were calculated with AutoGrid (part of the AutoDock package). The size of grid (one for each atom type in the ligand, plus one for electrostatic interactions) was set in a way to include not only the active site but also considerable portions of the surrounding surface. For this purpose, a grid of 60 × 60 × 60 points in x, y, and z directions was built centered on the center of mass of the catalytic site of β-secretase with a spacing of 0.375 Å. Cluster analysis was performed on the docked results using an RMSD tolerance of 2 Å.

Schematic 2D representations of the ligand-receptor interactions were all generated using LIGPLOT.<sup>44</sup>

#### 4.1.2. Ab initio study

Detailed analysis of ligand-receptor interactions were performed using amino acid decomposition analysis (ADA). The contribution of individual ligand-amino acid interaction energies in total binding energy was estimated using this method. Previously, ADA has been applied by our group in analyzing BACE-1 interactions with an isophthalamide-based scaffold.<sup>34</sup>

Amino acid residues involved in binding of 1,4-DHP ligands to the BACE-1 active site were chosen as a model on the basis of obtained ligand-receptor binding profiles and various crystallographic data (<http://www.rcsb.org/>). For this purpose, all involved amino acids (residues) were considered in their real electrostatic state. Each residue was truncated in its C and N terminals.

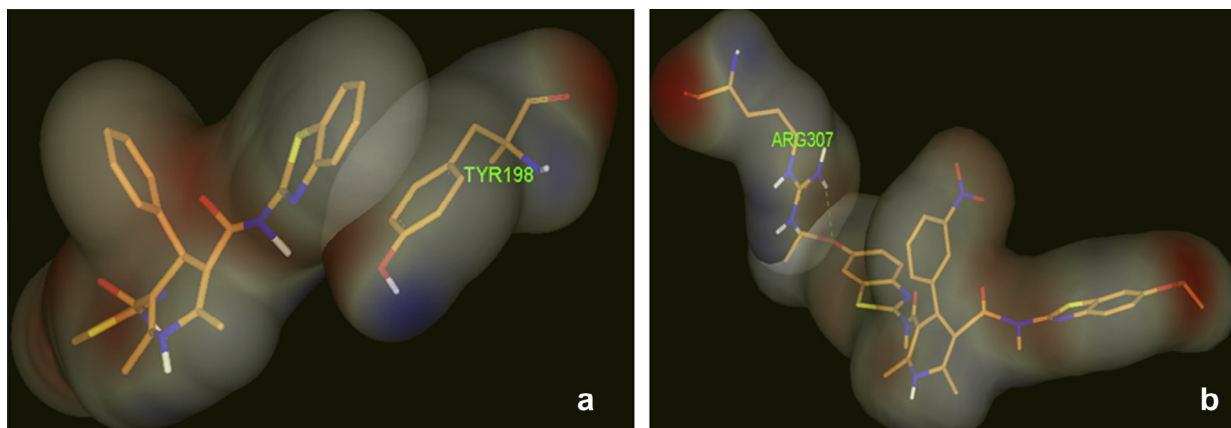
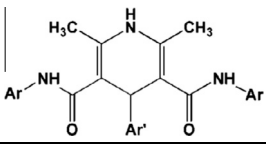


**Figure 7.** (a) Nearly parallel orientated aromatic rings of **6m** and Tyr198 and possible  $\pi$ - $\pi$  stacking interaction, (b) Extended  $\pi$ -acceptor substituted aromatic ring of **6i** supported H-bond interaction with Arg307 in the S4 subpocket.

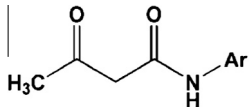
**Table 6**  
Calcium channel antagonist activities (IC<sub>50</sub>) of compounds **6a**, **6d**, **6k** and **6n**

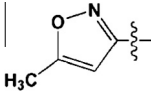
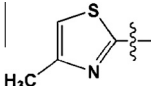
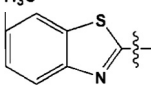
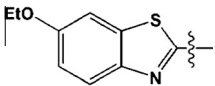


IC <sub>15</sub> (M)	IC <sub>30</sub> <sup>a</sup> (M)	Ar'	Ar	Compd. code
$(2.26 \pm 1.19) \times 10^{-6}$	$10^{-5} <$	2-furyl	4-methyl-2-thiazolyl	<b>6a</b>
$(4.63 \pm 1.43) \times 10^{-6}$	$(2.66 \pm 1.35) \times 10^{-5}$	4-nitrophenyl	4-methyl-2-thiazolyl	<b>6d</b>
$(6.47 \pm 1.46) \times 10^{-7}$	$(3.48 \pm 0.97) \times 10^{-6}$	2-nitrophenyl	2-benzothiazolyl	<b>6k</b>
$(1.82 \pm 0.45) \times 10^{-6}$	$10^{-5} <$	2-nitrophenyl	4-methyl-2-thiazolyl	<b>6n</b>
$(2.02 \pm 0.76) \times 10^{-9}$	$(9.27 \pm 1.24) \times 10^{-9}$	–	–	Nifedipine

<sup>a</sup> Muscle relaxation effects have been reported as the average of at least 3 trials ( $\pm$ S.E.).

**Table 7**  
Physical and analytical data of intermediates (**3a–e**)



Compd.	Substituent Ar	Mol. formula (Mol. Wt.)	mp <sup>a</sup> (°C)	Yield <sup>a</sup> (%)
<b>3a</b>		C <sub>7</sub> H <sub>8</sub> N <sub>2</sub> O <sub>2</sub> S (184.03)	158–160	89
<b>3b</b>		C <sub>8</sub> H <sub>10</sub> N <sub>2</sub> O <sub>3</sub> (182.07)	120–121	91
<b>3c</b>		C <sub>8</sub> H <sub>10</sub> N <sub>2</sub> O <sub>2</sub> S (198.05)	173–175	86
<b>3d</b>		C <sub>11</sub> H <sub>10</sub> N <sub>2</sub> O <sub>2</sub> S (234.05)	214–216	65
<b>3e</b>		C <sub>13</sub> H <sub>14</sub> N <sub>2</sub> O <sub>3</sub> S (278.07)	206–208	41

<sup>a</sup> Isolated yield.

To mimic the original electron density, N-terminal was acetylated and C-terminal was methyl amidated. All conformational and configurational features were held as original X-ray structure. Hydrogen bonds are not clearly recognized in a typical X-ray crystallographic file, and due to this limitation, we further optimized the heavy atom-hydrogen bonds by B3LYP/TZV (2d,2p) method using heavy atom fixing (HAF) approximation (constrained optimizations).<sup>45</sup> Constrained optimization was used to prevent irrational movement of the side chains.<sup>46</sup> All the interaction energies were estimated by the same method and basis set. In energy calculations, long-range dielectric effects of protein were considered using COSMO model<sup>36</sup> with a dielectric constant of 4.8.<sup>47</sup> The whole calculations were done with the ORCA quantum chemistry package.<sup>48</sup>

## 4.2. Chemistry

All the reagents were purchased from Merck chemical company and used without further purification. Nano particles of Fe<sub>3</sub>O<sub>4</sub> were prepared according to the co-precipitation procedure and were freshly used.<sup>49</sup> Prepared super paramagnetic nanoparticles (Fe<sub>3</sub>O<sub>4</sub>) were characterized by transmission electron microscopy (TEM) (Philips), the zeta-potential particle size distributing method (Horiba LB-550) and FT-IR spectrum (Nicolet FT-IR Magna 550).

Melting points were determined with a Reichert-Jung hot-stage microscope and were uncorrected. FT-IR (KBr) spectra were recorded on a Nicolet FT-IR Magna 550 spectrophotometer. <sup>1</sup>H NMR spectra were determined by a Bruker FT-500 MHz spectrometer in chloroform-*d*<sub>1</sub> or DMSO-*d*<sub>6</sub>. All the chemical shifts were reported as ( $\delta$ ) values (ppm) against tetramethylsilane as an internal standard. The MS spectra were recorded using Agilent 7890A spectrometer at 70 eV. CHN/CHNS analysis was performed using CHNS-932 Leco analyzer and the results were within  $\pm$  0.4% of the theoretical values.

The progress of the reactions and purity of the products were checked by analytical thin-layer chromatography (TLC) on pre-coated silica gel 60 F254 aluminum plates (Merck, Germany). Preparative column chromatographies were carried out on silica gel (230–400 mesh, G60 Merck). Preparative thin-layer chromatography was done with prepared glass-backed plates (20  $\times$  20 cm<sup>2</sup>, 500  $\mu$ ) using silica gel (Merk Kieselgel 60 HF254, Art. 7739).

### 4.2.1. General procedure for the synthesis of *N*-(aryl)-3-oxobutanamides (**3a–e**)

*N*-(Aryl)-3-oxobutanamides (**3a–e**) were synthesized according to the modified method of Clemens via condensation of 2,2,6-trimethyl-1,3-dioxine-4-one with the appropriate arylamine.<sup>50</sup> The results are represented in Table 7.

**4.2.1.1. N-(2-Thiazolyl) 3-oxo-butanamide (3a).** Pale yellow crystals; Yield 89%;  $^1\text{H NMR}$  (DMSO- $d_6$ )  $\delta$  (ppm) 11.32 (s, 2H, NH-amide), 8.93 (s, 1H, NH-DHP), 7.46 (d,  $J = 4$  Hz, 1H, CH-furyl), 6.71 (t,  $J = 3.6$  Hz, 1H, CH-furyl), 6.40 (s, 2H, CH<sub>3</sub>-thiazole), 5.90 (d,  $J = 3.2$  Hz, 1H, CH-furyl), 5.34 (s, 1H, C4H-DHP), 2.29 (s, 6H, CH<sub>3</sub>-thiazole), 2.25 (s, 6H, CH<sub>3</sub>-DHP); IR (KBr)  $\nu$  (cm<sup>-1</sup>): 3344.4 (N-H, DHP), 2924.0 (C-H, aliphatic), 1667.6 (C=O, amide), 1598.3 (C=C, alkene); MS  $m/z$  (%): 455(35) [M<sup>+</sup>], 410(12), 399(50), 313(75), 228(79), 202(100), 115(85), 42(21); Anal. Calcd (%) for C<sub>7</sub>H<sub>8</sub>N<sub>2</sub>O<sub>2</sub>S: C, 45.64; H, 4.38; N, 15.21; S, 17.41. Found: C, 45.78; H, 4.44; N, 15.26; S, 17.34.

**4.2.1.2. N-(5-Methyl-3-isoxazolyl)-3-oxobutanamide (3b).** Pale yellow crystals; yield 91%;  $^1\text{H NMR}$  (DMSO- $d_6$ )  $\delta$  (ppm) 10.49 (br s, 1H, NH-amide), 6.43 (s, 1H, C4H-isoxazole), 3.59 (s, 2H, COCH<sub>2</sub>CO), 2.37 (s, 3H, CH<sub>3</sub>CO), 2.18 (s, 3H, CH<sub>3</sub>-isoxazole); IR (KBr)  $\nu$  (cm<sup>-1</sup>): 3265.1 (N-H, amide), 3089.5 (C-H, aromatic), 2979.0 and 2934.7 (C-H, aliphatic), 1729.3 (C=O, ketone), 1673.8 (C=O, amide); MS  $m/z$  (%): 182(35) [M<sup>+</sup>], 140(12), 125(14), 98(100), 43(79); Anal. Calcd (%) for C<sub>8</sub>H<sub>10</sub>N<sub>2</sub>O<sub>3</sub>: C, 52.74; H, 5.53; N, 15.38. Found: C, 52.69; H, 5.51; N, 15.46.

**4.2.1.3. N-(4-Methyl-2-thiazolyl)-3-oxobutanamide (3c).** Pale yellow crystals; Yield 86%;  $^1\text{H NMR}$  (DMSO- $d_6$ )  $\delta$  (ppm) 11.65 (br s, 1H, NH-amide), 7.26 (s, 1H, C5H-thiazole), 3.76 (s, 2H, COCH<sub>2</sub>CO), 2.35 (s, 3H, CH<sub>3</sub>CO), 2.21 (s, 3H, CH<sub>3</sub>-thiazole); IR (KBr)  $\nu$  (cm<sup>-1</sup>): 3179.8 (N-H, amide), 3053.0 (C-H, aromatic), 2974.2 and 2899.2 (C-H, aliphatic), 1723.5 (C=O, ketone), 1672.9 (C=O, amide);

MS  $m/z$  (%): 198(29) [M<sup>+</sup>], 141(8), 114(100), 72(23), 43(65); Anal. Calcd (%) for C<sub>8</sub>H<sub>10</sub>N<sub>2</sub>O<sub>2</sub>S: C, 48.47; H, 5.08; N, 14.13; S, 16.17. Found: C, 48.39; H, 5.14; N, 14.26; S, 16.30.

**4.2.1.4. N-(2-Benzothiazolyl)-3-oxobutanamide (3d).** Pale yellow crystals; Yield 65%;  $^1\text{H NMR}$  (DMSO- $d_6$ )  $\delta$  (ppm) 11.65 (br s, 1H, NH-amide), 7.86 (d,  $J = 7.6$  Hz, 1H, C4'-benzothiazole), 7.68 (d,  $J = 8.0$  Hz, 1H, C7'H-benzothiazole), 7.35 (t,  $J = 8.4$  Hz, 1H, C5'H-benzothiazole), 7.20 (t,  $J = 8.0$  Hz, 1H, C6'H-benzothiazole), 3.73 (s, 2H, COCH<sub>2</sub>CO), 2.23 (s, 3H, CH<sub>3</sub>CO); IR (KBr)  $\nu$  (cm<sup>-1</sup>): 3178.7 (N-H, amide), 3067.5 (C-H, aromatic), 2917.3 and 2859.2 (C-H, aliphatic), 1719.4 (C=O, ketone), 1661.3 (C=O, amide); MS  $m/z$  (%): 234(25) [M<sup>+</sup>], 177(6), 150(100), 123(11), 43(32); Anal. Calcd (%) for C<sub>11</sub>H<sub>10</sub>N<sub>2</sub>O<sub>2</sub>S: C, 56.39; H, 4.30; N, 11.96; S, 13.69. Found: C, 56.20; H, 4.42; N, 12.11; S, 13.52.

**4.2.1.5. N-(6-Ethoxy-2-benzothiazolyl)-3-oxobutanamide (3e).** Pale yellow crystals; Yield 41%;  $^1\text{H NMR}$  (DMSO- $d_6$ )  $\delta$  (ppm) 11.88 (br s, 1H, NH-amide), 7.62 (d,  $J = 8.8$  Hz, 1H, C4'H-benzothiazole), 7.54 (d,  $J = 2.4$  Hz, 1H, C7'H-benzothiazole), 7.01 (d,  $J = 8.8$  Hz, 1H, C5'H-benzothiazole), 4.06 (q,  $J = 6.8$  Hz, 2H, -OCH<sub>2</sub>CH<sub>3</sub>), 3.75 (s, 2H, COCH<sub>2</sub>CO), 2.23 (s, 3H, CH<sub>3</sub>CO), 1.35 (t,  $J = 6.4$  Hz, 3H, -OCH<sub>2</sub>CH<sub>3</sub>); IR (KBr)  $\nu$  (cm<sup>-1</sup>): 3190.2 (N-H, amide), 3085.8 (C-H, aromatic), 2962.5 and 2889.6 (C-H, aliphatic), 1720.6 (C=O, ketone), 1661.9 (C=O, amide); MS  $m/z$  (%): 278(58) [M<sup>+</sup>], 220(18), 194(100), 165(86), 43(41); Anal. Calcd (%) for C<sub>13</sub>H<sub>14</sub>N<sub>2</sub>O<sub>3</sub>S: C, 56.10; H, 5.07; N, 10.06; S, 11.52. Found: C, 56.23; H, 4.95; N, 10.18; S, 11.41.

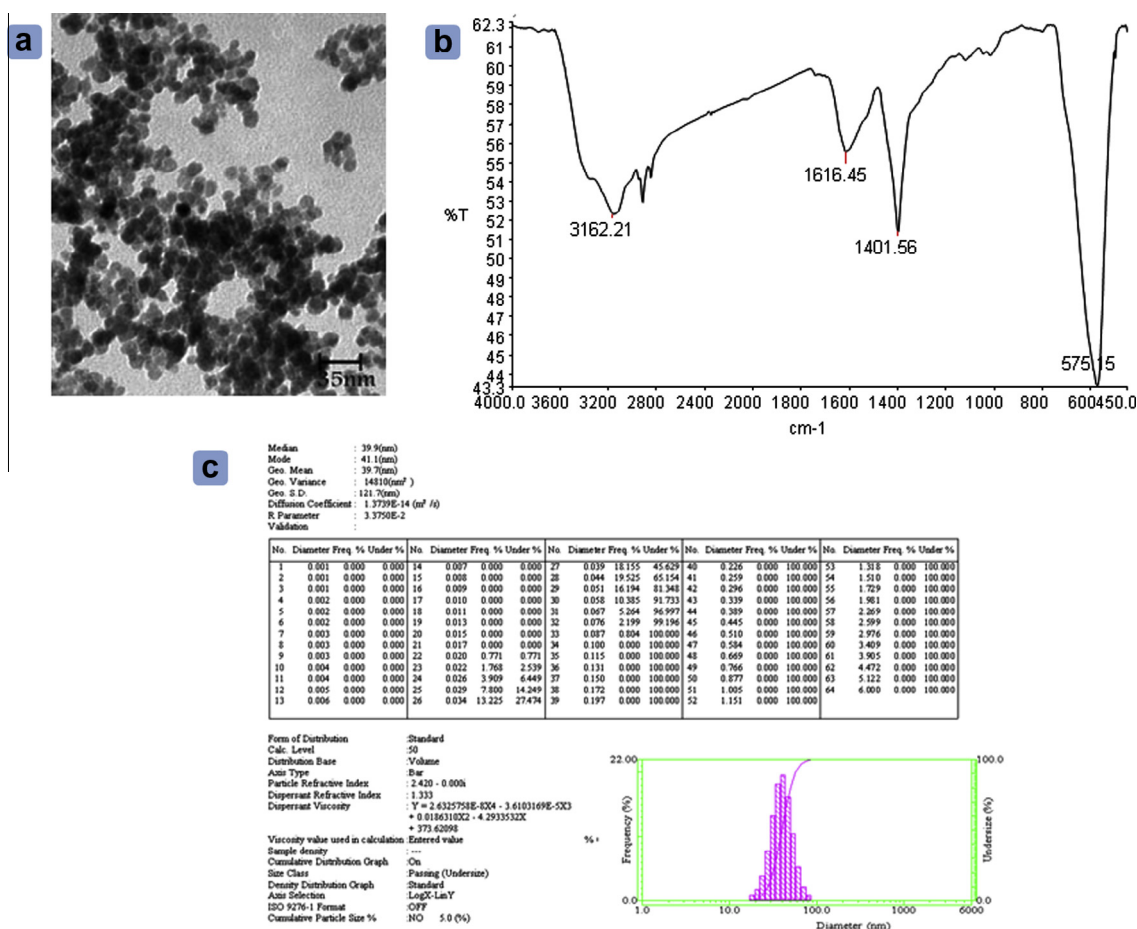


Figure 8. Characterization of prepared nano-Fe<sub>3</sub>O<sub>4</sub> nano particles by (a) TEM, (b) FTIR and (c) particle size analyzing methods.

#### 4.2.2. Preparation of superparamagnetic Fe<sub>3</sub>O<sub>4</sub> nanoparticles

Fe<sub>3</sub>O<sub>4</sub> nanoparticles were prepared using co-precipitation method.<sup>49</sup> The average particle size was found to be 39.9 nm. The characterization of Nano Fe<sub>3</sub>O<sub>4</sub> particles was performed via TEM, particle size analyzer and FTIR spectra<sup>51</sup> (Fig. 8).

#### 4.2.3. General procedure for the synthesis of 2,6-dimethyl-3,5-bis-N-(aryl) carbamoyl-4-aryl-1,4-dihydropyridines (6a–p)

**Conventional method:** A mixture of aldehyde **4** (1 mmol), corresponding *N*-arylacetoacetamide **3a–e** (2 mmol) and ammonium acetate **5** (2 mmol) was refluxed in 20 mL absolute ethanol in an oil bath for 24–48 h. The progress of the reaction was monitored by TLC. On completion of the reaction, the solvent was removed to some extent under reduced pressure. The product was filtered, washed with small portions of cold methanol and then dried. Further purification by column chromatography or/and preparative TLC using ethylacetate/petroleum ether as eluent followed by re-crystallization from appropriate solvent(s) gave pure compounds **6a–p**.

**Nano-Fe<sub>3</sub>O<sub>4</sub> catalyzed:** To a stirred suspension of nano-iron oxide (20 mol%) in absolute ethanol (25 mL) were added aldehyde **4** (1 mmol), *N*-arylacetoacetamide **3a–e** (2 mmol) and ammonium acetate **5** (2 mmol). The mixture was stirred and heated for desired period while the completion of the reaction was monitored by TLC. After completion of the reaction, nano iron oxides were separated using a super-magnet. Preparative TLC in ethyl acetate/petroleum ether eluent gave the pure DHP compounds. Further purification process was done via re-crystallization in appropriate solvent(s).

Obtained DHP compounds were characterized by IR, MS and <sup>1</sup>H NMR spectra along with CHN/CHNS analysis. Physical and characteristic data of the final compounds are summarized in Table 8.

Characteristic data for synthesized DHP derivatives are as follows:

##### 4.2.2.1. 2,6-Dimethyl-3,5-bis-N-(4-methyl-2-thiazolyl) carbamoyl-4-(2-furyl)-1,4-dihydropyridine (6a).

Pale yellow precipitates; Yield 32%; <sup>1</sup>H NMR (DMSO-*d*<sub>6</sub>) δ (ppm) 11.32 (s, 2H, NH-amide), 8.93 (s, 1H, NH-DHP), 7.46 (d, *J* = 4 Hz, 1H, CH-furyl), 6.71 (t, *J* = 3.6 Hz, 1H, CH-furyl), 6.40 (s, 2H, CH-thiazole), 5.90 (d, *J* = 3.2 Hz, 1H, CH-furyl), 5.34 (s, 1H, C4H-DHP), 2.29 (s, 6H, CH<sub>3</sub>-thiazole), 2.25 (s, 6H, CH<sub>3</sub>-DHP); IR (KBr) ν (cm<sup>-1</sup>): 3344.4 (N–H, DHP), 2924.0 (C–H, aliphatic), 1667.6 (C=O, amide), 1598.3 (C=C, alkene); MS *m/z* (%): 455(35) [M<sup>+</sup>], 410(12), 399(50), 313(75), 228(79), 202(100), 115(85), 42(21); Anal. Calcd (%) for C<sub>21</sub>H<sub>21</sub>N<sub>5</sub>O<sub>3</sub>S<sub>2</sub>: C, 55.37; H, 4.65; N, 15.37, S, 14.08. Found: C, 55.26; H, 4.51; N, 15.28; S, 14.17.

##### 4.2.2.2. 2,6-Dimethyl-3,5-bis-N-(2-thiazolyl) carbamoyl-4-(4-nitrophenyl)-1,4-dihydropyridine (6b).

Yellow crystals; Yield 32%; <sup>1</sup>H NMR (DMSO-*d*<sub>6</sub>) δ (ppm) 11.74 (s, 2H, NH-amide), 8.92 (s, 1H, NH-DHP), 8.14 (d, *J* = 8.8 Hz, 2H, CH-phenyl), 7.49 (d, *J* = 3.2 Hz, 2H, C4'H-thiazole), 7.38 (d, *J* = 8.8 Hz, 2H, CH-phenyl), 7.17 (d, *J* = 3.6, 2H, Hz, C5'H-thiazole), 5.43 (s, 1H, C4H-DHP), 2.23 (s, 6H, CH<sub>3</sub>-DHP); IR (KBr) ν (cm<sup>-1</sup>): 3345.9 (N–H, DHP), 2921.3 (C–H, aliphatic), 1676.2 (C=O, amide), 1647.8 (C=C, alkene); MS *m/z* (%): 482(12) [M<sup>+</sup>], 465 (100), 381(18), 339(11), 255(31), 101(33), 91(42), 55(12); Anal. Calcd (%) for C<sub>21</sub>H<sub>18</sub>N<sub>6</sub>O<sub>4</sub>S<sub>2</sub>: C, 52.27; H, 3.76; N, 17.42; S, 13.29. Found: C, 52.10; H, 4.91; N, 17.41; S, 13.46.

##### 4.2.2.3. 2,6-Dimethyl-3,5-bis-N-(5-methyl-3-isoxazolyl) carbamoyl-4-(4-nitrophenyl)-1,4-dihydropyridine (6c).

Yellow crystals; Yield 16%; <sup>1</sup>H NMR (CDCl<sub>3</sub>) δ (ppm) 8.17 (d, *J* = 8.5 Hz, 2H, CH-phenyl), 7.85 (s, 2H, NH-amide), 7.50 (d, *J* = 8.5 Hz, 2H, CH-phenyl), 6.64 (s, 2H, C4'H-isoxazole), 5.62 (s, 1H, NH-DHP), 5.03 (s, 1H, C4H-DHP), 2.38 (s, 6H, CH<sub>3</sub>-isoxazole), 2.33 (s, 6H, CH<sub>3</sub>-DHP); IR (KBr) ν (cm<sup>-1</sup>): 3244.1 (N–H, DHP), 3107.9 (N–H, amide), 2920.9 (C–H, aliphatic), 1692.1 (C=O, amide), 1643.8,

**Table 8**  
Physical and analytical data of 1,4-DHPs (**6a–p**)

Compd.	Ar'	Ar	Mol. formula (Mol. wt)	mp (°C)	Conventional method <sup>a</sup> yield <sup>b</sup> (%) / period (h)	Nano-Fe <sub>3</sub> O <sub>4</sub> catalyzed method <sup>c</sup> yield <sup>d</sup> (%) / period (h)
<b>6a</b>	4-Methyl-2-thiazolyl	2-Furyl	C <sub>21</sub> H <sub>21</sub> N <sub>5</sub> O <sub>3</sub> S <sub>2</sub> 455.11	194–196	32 (48)	79 (4)
<b>6b</b>	2-Thiazolyl	4-Nitrophenyl	C <sub>21</sub> H <sub>18</sub> N <sub>6</sub> O <sub>4</sub> S <sub>2</sub> 482.08	159–161	26 (24)	81 (1)
<b>6c</b>	5-Methyl-3-isoxazolyl	4-Nitrophenyl	C <sub>23</sub> H <sub>22</sub> N <sub>6</sub> O <sub>6</sub> 478.16	240–242	16 (24)	69 (8)
<b>6d</b>	4-Methyl-2-thiazolyl	4-Nitrophenyl	C <sub>23</sub> H <sub>22</sub> N <sub>6</sub> O <sub>4</sub> S <sub>2</sub> 510.11	206–208	33 (28)	73 (7)
<b>6e</b>	2-Benzothiazolyl	4-Nitrophenyl	C <sub>29</sub> H <sub>22</sub> N <sub>6</sub> O <sub>4</sub> S <sub>2</sub> 582.11	209–211	35 (24)	83 (1)
<b>6f</b>	5-Methyl-3-isoxazolyl	3-Nitrophenyl	C <sub>23</sub> H <sub>22</sub> N <sub>6</sub> O <sub>6</sub> 478.16	243–245	17 (24)	61 (9)
<b>6g</b>	4-Methyl-2-thiazolyl	3-Nitrophenyl	C <sub>23</sub> H <sub>22</sub> N <sub>6</sub> O <sub>4</sub> S <sub>2</sub> 510.11	162–164	31 (24)	65 (5)
<b>6h</b>	2-Benzothiazolyl	3-Nitrophenyl	C <sub>29</sub> H <sub>22</sub> N <sub>6</sub> O <sub>4</sub> S <sub>2</sub> 582.11	202–204	37 (36)	77 (6)
<b>6i</b>	6-Ethoxy-2-benzothiazolyl	3-Nitrophenyl	C <sub>33</sub> H <sub>30</sub> N <sub>6</sub> O <sub>6</sub> S <sub>2</sub> 670.17	160–162	24 (40)	68 (4)
<b>6j</b>	5-Methyl-3-isoxazolyl	2-Nitrophenyl	C <sub>23</sub> H <sub>22</sub> N <sub>6</sub> O <sub>6</sub> 478.16	209–211	11 (48)	66 (6)
<b>6k</b>	2-Benzothiazolyl	2-Nitrophenyl	C <sub>29</sub> H <sub>22</sub> N <sub>6</sub> O <sub>4</sub> S <sub>2</sub> 582.11	214–216	31 (30)	81 (4)
<b>6l</b>	5-Methyl-3-isoxazolyl	2-Pyrrolyl	C <sub>21</sub> H <sub>22</sub> N <sub>6</sub> O <sub>4</sub> 422.17	136–137	16 (48)	62 (6)
<b>6m</b>	2-Benzothiazolyl	Phenyl	C <sub>29</sub> H <sub>23</sub> N <sub>5</sub> O <sub>2</sub> S <sub>2</sub> 537.13	182–184	21 (24)	76 (3)
<b>6n</b>	4-Methyl-2-thiazolyl	2-Nitrophenyl	C <sub>23</sub> H <sub>22</sub> N <sub>6</sub> O <sub>4</sub> S <sub>2</sub> 510.11	177–180	28 (24)	78 (4)
<b>6o</b>	4-Methyl-2-thiazolyl	4-Methoxyphenyl	C <sub>24</sub> H <sub>25</sub> N <sub>5</sub> O <sub>3</sub> S <sub>2</sub> 495.14	151–153	23 (48)	71 (5)
<b>6p</b>	4-Methyl-2-thiazolyl	6-Methyl-2-pyridyl	C <sub>23</sub> H <sub>24</sub> N <sub>6</sub> O <sub>2</sub> S <sub>2</sub> 480.14	230–232	15 (48)	69 (3)

<sup>e</sup>PE: petroleum ether.

<sup>a</sup> Refluxing in EtOH for 24–48 h.

<sup>b</sup> Isolated yield.

<sup>c</sup> Refluxing in EtOH in the presence of nano-Fe<sub>3</sub>O<sub>4</sub>.

<sup>d</sup> Isolated yield.

1621.5, (C=C, alkene), 1519.7 and 1344.6 (C–NO<sub>2</sub> aromatic); MS *m/z* (%): 478(3) [M<sup>+</sup>], 463 (7), 379(25), 356(19), 255(56), 228(50), 182(37), 98(33), 43(100); Anal. Calcd (%) for C<sub>23</sub>H<sub>22</sub>N<sub>6</sub>O<sub>6</sub>: C, 57.74; H, 4.63; N, 17.56. Found: C, 57.88; H, 4.84; N, 17.41.

**4.2.2.4. 2,6-Dimethyl-3,5-bis-N-(4-methyl-2-thiazolyl) carbamoyl-4-(4-nitrophenyl)-1,4-dihydropyridine (6d).** Yellow precipitates; Yield 33%; <sup>1</sup>H NMR (CDCl<sub>3</sub>) δ (ppm) 10.25 (s, 2H, NH-amide), 8.09 (d, *J* = 8.3 Hz, 2H, CH-phenyl), 7.43 (d, *J* = 8.3 Hz, 2H, CH-phenyl), 6.48 (s, 2H, CH-thiazole), 5.91 (br s, 1H, NH-DHP), 5.41 (s, 1H, C4H-DHP), 2.43 (s, 6H, CH<sub>3</sub>-thiazole), 2.34 (s, 6H, CH<sub>3</sub>-DHP); IR (KBr) *v* (cm<sup>-1</sup>): 3311.1 (N–H, DHP), 3107.9 (N–H, amide), 2920.9 (C–H, aliphatic), 1670.5 (C=O, amide), 1604.7 (C=C, alkene), 1526.6 and 1348.6 (C–NO<sub>2</sub> aromatic); MS *m/z* (%): 510(3) [M<sup>+</sup>], 508(22), 395(67), 281(54), 255(100), 114(63); Anal. Calcd (%) for C<sub>23</sub>H<sub>22</sub>N<sub>6</sub>O<sub>4</sub>S<sub>2</sub>: C, 54.10; H, 4.34; N, 16.46; S, 12.56. Found: C, 53.98; H, 4.70; N, 16.61; S, 12.24.

**4.2.2.5. 2,6-Dimethyl-3,5-bis-N-(2-benzothiazolyl) carbamoyl-4-(4-nitrophenyl)-1,4-dihydropyridine (6e).** Yellow crystals; Yield 35%; <sup>1</sup>H NMR (CDCl<sub>3</sub>) δ (ppm) 10.21 (s, 2H, NH-amide), 8.11 (d, *J* = 8.1 Hz, 2H, CH-phenyl), 7.80 (d, *J* = 7.8 Hz, 2H, C4'H-benzothiazole), 7.74 (d, *J* = 7.8 Hz, 2H, C7'H-benzothiazole), 7.53 (d, *J* = 8.2 Hz, 2H, CH-phenyl), 7.46 (t, *J* = 7.4 Hz, 2H, C5'H-benzothiazole), 7.33 (t, *J* = 7.4 Hz, 2H, C6'H-benzothiazole), 5.97 (s, 1H, NH-DHP), 5.48 (s, 1H, C4H-DHP), 2.46 (s, 6H, CH<sub>3</sub>-DHP); IR (KBr) *v* (cm<sup>-1</sup>): 3332.9 (N–H, DHP), 2924 (C–H, aliphatic), 1655.4 (C=O, amide), 1598.2 (C=C, alkene), 1534.5 and 1345.9 (C–NO<sub>2</sub> aromatic); MS *m/z* (%): 582 (3) [M<sup>+</sup>], 580 (9), 431(24), 389(37), 255(89), 150(100); Anal. Calcd (%) for C<sub>29</sub>H<sub>22</sub>N<sub>6</sub>O<sub>4</sub>S<sub>2</sub>: C, 59.78; H, 3.81; N, 14.42; S, 11.01. Found: C, 59.68; H, 3.98; N, 14.61, S, 11.09.

**4.2.2.6. 2,6-Dimethyl-3,5-bis-N-(5-methyl-3-isoxazolyl) carbamoyl-4-(3-nitrophenyl)-1,4-dihydropyridine (6f).** Pale yellow crystals; Yield 17%; <sup>1</sup>H NMR (DMSO-*d*<sub>6</sub>) δ (ppm) 10.48 (s, 2H, NH-amide), 8.63 (br s, 1H, NH-DHP), 8.13 (s, 1H, CH-phenyl), 8.05 (d, *J* = 9 Hz, 1H, CH-phenyl), 7.99 (d, *J* = 9 Hz, 1H, CH-phenyl), 7.56 (t, *J* = 9.5 Hz, 1H, CH-phenyl), 6.57 (s, 2H, C4'H-isoxazole), 5.26 (s, 1H, C4H-DHP), 2.34 (s, 6H, CH<sub>3</sub>-isoxazole), 2.15 (s, 6H, CH<sub>3</sub>-DHP); IR (KBr) *v* (cm<sup>-1</sup>): 3331.8 (N–H, DHP), 1672.2 (C=O, amide), 1622.1 (C=C, alkene), 1523.8 and 1346.1 (C–NO<sub>2</sub> aromatic), 697.5, 788.2, 878 (*meta* substituted benzene); MS *m/z* (%): 478(11) [M<sup>+</sup>], 463 (100), 379(51), 356(95), 255(47), 232(77), 134(46), 43(100); Anal. Calcd (%) for C<sub>23</sub>H<sub>22</sub>N<sub>6</sub>O<sub>6</sub>: C, 57.74; H, 4.63; N, 17.56. Found: C, 57.77; H, 4.69; N, 17.41.

**4.2.2.7. 2,6-Dimethyl-3,5-bis-N-(4-methyl-2-thiazolyl) carbamoyl-4-(3-nitrophenyl)-1,4-dihydropyridine (6g).** Pale yellow precipitates; Yield 31%; <sup>1</sup>H NMR (CDCl<sub>3</sub>) δ (ppm) 10.11 (s, 2H, NH-amide), 8.14 (s, 1H, CH-phenyl), 8.01 (d, *J* = 8.2 Hz, 1H, CH-phenyl), 7.97 (d, *J* = 8.2 Hz, 1H, CH-phenyl), 7.40 (t, *J* = 7.5 Hz, 1H, CH-phenyl), 6.48 (s, 2H, CH-thiazole), 6.29 (br s, 1H, NH-DHP), 5.74 (s, 1H, C4H-DHP), 2.48 (s, 6H, CH<sub>3</sub>-thiazole), 2.37 (s, 6H, CH<sub>3</sub>-DHP); IR (KBr) *v* (cm<sup>-1</sup>): 3211.6 (N–H, DHP), 2923.9 (C–H, aliphatic), 1660.5 (C=O, amide), 1523.5, 1349.3 (C–NO<sub>2</sub>, aromatic); MS *m/z* (%): 510(8) [M<sup>+</sup>], 508(19), 493(64), 395(72), 255(100), 141(27), 114(67); Anal. Calcd (%) for C<sub>23</sub>H<sub>22</sub>N<sub>6</sub>O<sub>4</sub>S<sub>2</sub>: C, 54.10; H, 4.34; N, 16.46; S, 12.56. Found: C, 54.23; H, 4.41; N, 16.39; S, 12.50.

**4.2.2.8. 2,6-Dimethyl-3,5-bis-N-(2-benzothiazolyl) carbamoyl-4-(3-nitrophenyl)-1,4-dihydropyridine (6h).** Yellow crystals; Yield 37%; <sup>1</sup>H NMR (CDCl<sub>3</sub>) δ (ppm) 9.91 (s, 2H, NH-amide), 8.20 (s, 1H, CH-phenyl), 7.99 (d, *J* = 9 Hz, 1H, CH-phenyl), 7.78 (d, *J* = 7.45 Hz, 2H, C4'H-benzothiazole), 7.71 (br s, 3H, C7'H-benzothiazole and CH-phenyl), 7.45 (t, *J* = 7.5, 2H, C5'H-benzothiazole), 7.32 (t, *J* = 7.2 Hz, 3H, C6'H-benzothiazole and CH-phenyl), 6.00 (br s,

1H, NH-DHP), 5.29 (s, 1H, C4H-DHP), 2.39 (s, 6H, CH<sub>3</sub>-DHP); IR (KBr) *v* (cm<sup>-1</sup>): 3366.5 (N–H, DHP), 2926 (C–H, aliphatic), 1660.6 (C=O, amide), 1595.7 (C=C, alkene), 1530.8 and 1344.1 (C–NO<sub>2</sub> aromatic), 685.8, 759.1, 863.8 (*meta* substituted benzene); MS *m/z* (%): 582(5) [M<sup>+</sup>], 580(7), 431(10), 389(58), 255(78), 228(64), 176(58), 150(100); Anal. Calcd (%) for C<sub>29</sub>H<sub>22</sub>N<sub>6</sub>O<sub>4</sub>S<sub>2</sub>: C, 59.78; H, 3.81; N, 14.42; S, 11.01. Found: C, 59.83; H, 3.68; N, 14.56, S, 10.94.

**4.2.2.9. 2,6-Dimethyl-3,5-bis-N-(6-ethoxy-2-benzothiazolyl) carbamoyl-4-(3-nitrophenyl)-1,4-dihydropyridine (6i).** Yellow precipitates; Yield 24%; <sup>1</sup>H NMR (CDCl<sub>3</sub>) δ (ppm) 10.66 (s, 2H, NH-amide), 8.16 (s, 1H, CH-phenyl), 7.99 (d, *J* = 8.2 Hz, 1H, CH-phenyl), 7.83 (d, *J* = 7.1 Hz, 2H, CH-phenyl), 7.60 (d, *J* = 8.9 Hz, 2H, C4'H-benzothiazole), 7.37 (t, *J* = 8.0 Hz, 1H, CH-phenyl), 7.23 (t, *J* = 2.4 Hz, 2H, C7'H-benzothiazole), 7.04 (d, *J* = 8.8, 2H, C5'H-benzothiazole), 6.45 (br s, 1H, NH-DHP), 5.75 (s, 1H, C4H-DHP), 4.07 (q, *J* = 6.9 Hz, 4H, –OCH<sub>2</sub>CH<sub>3</sub>), 2.46 (s, 6H, CH<sub>3</sub>-DHP), 1.45 (t, *J* = 6.9 Hz, 6H, –OCH<sub>2</sub>CH<sub>3</sub>); IR (KBr) *v* (cm<sup>-1</sup>): 3373.3 (N–H, DHP), 2924.2 (C–H, aliphatic), 1662.2 (C=O, amide), 1605.5 (C=C, alkene); MS *m/z* (%): 670(9) [M<sup>+</sup>], 668(10), 475(19), 448(38), 255(78), 194(100), 165(94), 139(33); Anal. Calcd (%) for C<sub>33</sub>H<sub>30</sub>N<sub>6</sub>O<sub>6</sub>S<sub>2</sub>: C, 59.09; H, 4.51; N, 12.53; S, 9.56. Found: C, 59.19; H, 4.56; N, 12.44; S, 9.48.

**4.2.2.10. 2,6-Dimethyl-3,5-bis-N-(5-methyl-3-isoxazolyl) carbamoyl-4-(2-nitrophenyl)-1,4-dihydropyridine (6j).** Yellow precipitates; Yield 11%; <sup>1</sup>H NMR (CDCl<sub>3</sub>) δ (ppm) 8.69 (s, 2H, NH-amide), 7.70 (d, *J* = 8.0 Hz, 1H, CH-phenyl), 7.62 (t, *J* = 7.3 Hz, 1H, CH-phenyl), 7.55 (d, *J* = 7.2 Hz, 1H, CH-phenyl), 7.32 (t, *J* = 7.8 Hz, 1H, CH-phenyl), 6.59 (s, 2H, C4'H-isoxazole), 5.75 (s, 1H, NH-DHP), 5.64 (s, 1H, C4H-DHP), 2.36 (s, 6H, CH<sub>3</sub>-isoxazole), 2.25 (s, 6H, CH<sub>3</sub>-DHP); IR (KBr) *v* (cm<sup>-1</sup>): 3348.4 (N–H, DHP), 2924.2 (C–H, aliphatic), 1679.6 (C=O, amide), 1615.7 (C=C, alkene), 1527.4 and 1352.7 (C–NO<sub>2</sub> aromatic); MS *m/z* (%): 478(9) [M<sup>+</sup>], 461(100), 379(12), 334(29), 236(38), 182(8), 43(14); Anal. Calcd (%) for C<sub>23</sub>H<sub>22</sub>N<sub>6</sub>O<sub>6</sub>: C, 57.74; H, 4.63; N, 17.56; Found: C, 57.68; H, 4.78; N, 17.61.

**4.2.2.11. 2,6-Dimethyl-3,5-bis-N-(2-benzothiazolyl) carbamoyl-4-(2-nitrophenyl)-1,4-dihydropyridine (6k).** Yellow crystals; Yield 31%; <sup>1</sup>H NMR (CDCl<sub>3</sub>) δ (ppm) 10.46 (s, 2H, NH-amide), 7.91 (d, *J* = 7.5 Hz, 1H, CH-phenyl), 7.66–7.75 (m, 6H, C4'H, C5'H and C7'H-benzothiazole), 7.54 (t, *J* = 7.5 Hz, 1H, CH-phenyl), 7.39 (t, *J* = 7.5 Hz, 1H, CH-phenyl), 7.32 (m, 3H, C6'H-benzothiazole and CH-phenyl), 6.08 (s, 1H, NH-DHP), 5.93 (s, 1H, C4H-DHP), 2.51 (s, 6H, CH<sub>3</sub>-DHP); IR (KBr) *v* (cm<sup>-1</sup>): 3300.4 (N–H, DHP), 2922.1 (C–H, aliphatic), 1663.5 (C=O, amide), 1598.8 (C=C, alkene), 1525.9 and 1350.3 (C–NO<sub>2</sub> aromatic); MS *m/z* (%): 582 (5) [M<sup>+</sup>], 580 (43), 567(28), 431(81), 389(73), 370(32), 267(68), 150(100); Anal. Calcd (%) for C<sub>29</sub>H<sub>22</sub>N<sub>6</sub>O<sub>4</sub>S<sub>2</sub>: C, 59.78; H, 3.81; N, 14.42; S, 11.01. Found: C, 59.97; H, 3.88; N, 14.36, S, 11.12.

**4.2.2.12. 2,6-Dimethyl-3,5-bis-N-(5-methyl-3-isoxazolyl) carbamoyl-4-(2-pyrrolyl)-1,4-dihydropyridine (6l).** Pale yellow precipitates; Yield 16%; <sup>1</sup>H NMR (CDCl<sub>3</sub>) δ (ppm) 9.50 (br s, 1H, NH-pyrrol), 8.29 (s, 2H, NH-amide), 6.78 (Apparent br s, 1H, CH-pyrrol), 6.68 (s, 2H, C4'H-isoxazole), 6.09 (br s, 1H, NH-DHP), 6.00 (Apparent br s, 1H, CH-pyrrol), 5.83 (Apparent s, 1H, CH-pyrrol), 4.66 (s, 1H, C4H-DHP), 2.39 (s, 6H, CH<sub>3</sub>-isoxazole), 2.29 (s, 6H, CH<sub>3</sub>-DHP); IR (KBr) *v* (cm<sup>-1</sup>): 3318.01 (N–H, DHP), 2924.2 (C–H, aliphatic), 1669.7 (C=O, amide), 1615.4 (C=C, alkene); MS *m/z* (%): 422(5) [M<sup>+</sup>], 407(25), 340(67), 258(100), 225(28), 16(18), 43(22); Anal. Calcd (%) for C<sub>21</sub>H<sub>22</sub>N<sub>6</sub>O<sub>4</sub>: C, 59.71; H, 5.25; N, 19.89. Found: C, 59.63; H, 5.28; N, 19.69.

**4.2.2.13. 2,6-Dimethyl-3,5-bis-N-(2-benzothiazolyl) carbamoyl-4-phenyl-1,4-dihydropyridine (6m).** Pale yellow precipitates;

Yield 16%;  $^1\text{H}$  NMR ( $\text{CDCl}_3$ )  $\delta$  (ppm) 9.77 (s, 2H, NH-amide), 7.76 (2H, d,  $J = 9$  Hz, C4'H-benzothiazole), 7.66 (2H, d,  $J = 9$  Hz, C7'H-benzothiazole), 7.48 (2H, d,  $J = 7.4$  Hz, CH-phenyl), 7.31–7.42 (7H, m, CH-phenyl and C5'H and C6'H-benzothiazole), 5.85 (1H, s, NH-DHP), 5.06 (1H, s, C4H-DHP), 2.40 (6H, s,  $\text{CH}_3$ -DHP); IR (KBr)  $\nu$  ( $\text{cm}^{-1}$ ): 3338.5 (N–H, DHP), 2923.7 (C–H, aliphatic), 1666.7 (C=O, amide), 1598.5 (C=C, alkene); MS  $m/z$  (%): 537(5) [ $\text{M}^+$ ], 535(8), 389(10), 361(27), 236(24), 212(71), 183(100), 150(83), 115(23); Anal. Calcd (%) for  $\text{C}_{29}\text{H}_{23}\text{N}_5\text{O}_2\text{S}_2$ : C, 64.78; H, 4.31; N, 13.03; S, 11.93. Found: C, 64.67; H, 4.40; N, 13.31; S, 11.79.

**4.2.2.14. 2,6-Dimethyl-3,5-bis-*N*-(4-methyl-2-thiazolyl) carbamoyl-4-(2-nitrophenyl)-1,4-dihydropyridine (6n).** Yellow crystals; Yield 28%;  $^1\text{H}$  NMR ( $\text{CDCl}_3$ )  $\delta$  (ppm) 10.09 (s, 2H, NH-amide), 7.67 (d,  $J = 8.0$  Hz, 2H, CH-phenyl), 7.63 (d,  $J = 7.9$  Hz, 1H, CH-phenyl), 7.52 (t,  $J = 7.6$  Hz, 1H, CH-phenyl), 7.30 (t,  $J = 7.6$  Hz, 1H, CH-phenyl), 6.47 (s, 2H, CH-thiazole), 6.12 (br s, 1H, NH-DHP), 5.82 (s, 1H, C4H-DHP), 2.52 (s, 6H,  $\text{CH}_3$ -thiazole), 2.36 (s, 6H,  $\text{CH}_3$ -DHP); IR (KBr)  $\nu$  ( $\text{cm}^{-1}$ ): 3360.6 (N–H, DHP), 2923.3 (C–H, aliphatic), 1665.5 (C=O, amide), 1607.9 (C=C, alkene), 1525.2 and 1354.6 (C- $\text{NO}_2$  aromatic); MS  $m/z$  (%): 510(9) [ $\text{M}^+$ ], 493(70), 395(44), 353(90), 267(55), 210(86), 141(54), 114(100); Anal. Calcd (%) for  $\text{C}_{23}\text{H}_{22}\text{N}_6\text{O}_4\text{S}_2$ : C, 54.10; H, 4.34; N, 16.46. Found: C, 53.99; H, 4.99; N, 16.31.

**4.2.2.15. 2,6-Dimethyl-3,5-bis-*N*-(4-methyl-2-thiazolyl) carbamoyl-4-(4-methoxyphenyl)-1,4-dihydropyridine (6o).** Pale yellow precipitates; Yield 23%;  $^1\text{H}$  NMR ( $\text{DMSO}-d_6$ )  $\delta$  (ppm) 11.54 (s, 2H, NH-amide), 8.74 (s, 1H, NH-DHP), 7.02 (d,  $J = 8.8$  Hz, 2H, CH-phenyl), 6.79 (d,  $J = 8.8$  Hz, 2H, CH-phenyl), 6.69 (s, 2H, CH-thiazole), 5.18 (s, 1H, C4H-DHP), 3.64 (s, 3H,  $-\text{OCH}_3$ ), 2.29 (s, 6H, N- $\text{CH}_3$ ), 2.21 (s, 6H,  $\text{CH}_3$ -DHP); IR (KBr)  $\nu$  ( $\text{cm}^{-1}$ ): 3356.7 (N–H, DHP), 2924.3 (C–H, aliphatic), 1667.1 (C=O, amide), 1608.9 (C=C, alkene); MS  $m/z$  (%): 495(12) [ $\text{M}^+$ ], 493 (17), 380(46), 354(20), 266(100), 240(45), 115(31); Anal. Calcd (%) for  $\text{C}_{24}\text{H}_{25}\text{N}_5\text{O}_3\text{S}_2$ : C, 58.16; H, 5.08; N, 14.13; S, 12.94. Found: C, 58.27; H, 4.99; N, 14.31; S, 12.79.

**4.2.2.16. 2,6-Dimethyl-3,5-bis-*N*-(4-methyl-2-thiazolyl) carbamoyl-4-(6-methyl-2-pyridyl)-1,4-dihydropyridine (6p).** Pale yellow crystals; Yield 15%;  $^1\text{H}$  NMR ( $\text{CDCl}_3$ )  $\delta$  (ppm) 10.26 (br s, 2H, NH-amide), 7.67 (t,  $J = 7.5$  Hz, 1H, CH-pyridyl), 7.11 (d,  $J = 7.6$  Hz, 1H, CH-pyridyl), 7.07 (d,  $J = 7.4$  Hz, 1H, CH-pyridyl), 6.63 (s, 2H, CH-thiazole), 6.21 (br s, 1H, NH-DHP), 4.91 (s, 1H, C4H-DHP), 2.75 (s, 3H,  $\text{CH}_3$ -pyridyl), 2.39 (s, 6H,  $\text{CH}_3$ -thiazole), 2.36 (s, 6H,  $\text{CH}_3$ -DHP); IR (KBr)  $\nu$  ( $\text{cm}^{-1}$ ): 3355.2 (N–H, DHP), 2922.9 (C–H, aliphatic), 1665.8 (C=O, amide), 1594.3 (C=C, alkene); MS  $m/z$  (%): 480(5) [ $\text{M}^+$ ], 388(39), 366(100), 274(15), 225(85), 115(23), 42(7); Anal. Calcd (%) for  $\text{C}_{23}\text{H}_{24}\text{N}_6\text{O}_2\text{S}_2$ : C, 57.48; H, 5.03; N, 17.49; S, 13.34. Found: C, 57.27; H, 4.96; N, 17.41; S, 13.28.

### 4.3. Biological assessment

#### 4.3.1. BACE-1 inhibition assay

All synthesized compounds (6a-p) were evaluated for their BACE-1 inhibitory activity using a fluorescence resonance energy transfer (FRET) assay with recombinant human BACE-1 and quenched fluorescent peptide substrate based on the Swedish mutant APP sequence (SEVNLDAEFK). FRET-based enzymatic kit was purchased from Invitrogen (former Pan Vera corporation, Madison, WI) and the assay was carried out according to the manufacturers' instructions (Invitrogen. <http://tools.invitrogen.com/content/sfs/manuals/L0724.pdf>) using a multiplate spectrofluorometer instrument (Recording fluorescence at 544 nm excitation and 590 nm emission wavelengths) (BMG LABTECH, Polar star, Germany).

The assay procedure was as follows; the provided BACE-1 (purified baculovirus-expressed) and the peptide substrate (Rh-EVNLDAEFK-Quencher) were diluted in BACE-1 assay buffer (50 mM sodium acetate, pH 4.5) to obtain 3X solutions. Stock solutions of inhibitors in DMSO were diluted in assay buffer to provide 3X solution of test compounds at different concentrations. The final concentration of DMSO was kept under 4%. BACE-1 enzyme and test samples (10  $\mu\text{l}$  of each) were introduced into the 96-well plate while gently mixing. Then, BACE-1 substrate (10  $\mu\text{l}$ ) was added to the mixture and the plates were incubated at 25  $^\circ\text{C}$  for 90 min in the dark and then the reaction was stopped with 2.5 M sodium acetate (stop solution). Fluorescence was recorded at 544 nm (excitation) and 590 nm (emission) wavelengths to monitor the hydrolysis of the substrate. OM99-2 (Glu-Val-Asn-Leu- $\Psi$ -Ala-Ala-Glu-Phe, Calbiochem) was used as a reference inhibitor.

The percentages of enzyme inhibition for each concentration of tested compounds were calculated regarding the maximum enzyme activity wells (containing substrate plus enzyme) and baseline wells (containing substrate).  $\text{IC}_{50}$  values were calculated with CurveExpert software version 1.34 for Windows. Each experiment was repeated for three to four times. All data were presented as mean  $\pm$  S.E.

#### 4.3.2. Calcium channel blocking activity

Male albino guinea pigs (300–450 g) were purchased from animal house department of Shiraz University of Medical Sciences. They had free access to standard rodent chow and tap water at all times. The animals were housed at  $23 \pm 2$   $^\circ\text{C}$  temperature,  $55 \pm 10\%$  humidity, and on a 12 h light/dark cycle. The feeding was disrupted 1 day before starting in vitro tests. The animals were sacrificed by a blow to the head. The intestine was removed above the ileocecal junction and longitudinal smooth muscle segments of 2 cm length were mounted under a resting tension of 0.5 g. The segments were maintained at 37  $^\circ\text{C}$  in a 20 ml jacketed organ bath containing oxygenated physiological saline solution with the following composition (mM): NaCl 137,  $\text{CaCl}_2$  1.8, KCl 2.7,  $\text{MgSO}_4$  1.1,  $\text{NaH}_2\text{PO}_4$  0.4,  $\text{NaHCO}_3$  12 and glucose 5. The muscle was equilibrated for 1 h with a solution varying every 15 min. The contractions were recorded with a force displacement transducer (F-50) on a Narco Physiograph (Narco Biosystems, Houston, TX, USA). Test agents were prepared as 2–10 M stock solutions in DMSO and stored away from light. Dilutions were made with DMSO. The contractile response was taken as the 100% value for the tonic (slow) component of the response. The contraction was elicited with 40 mM KCl. Test compounds were cumulatively added and compound-induced relaxation of contracted muscle was expressed as percentage of control. Nifedipine was used as the reference compound. The  $\text{IC}_{30}$  values (concentration needed to produce 30% relaxation on contracted ileal smooth muscle) were graphically determined using Curve Expert 1.34 program. Data were expressed as means  $\pm$  SE. The one-way analysis of variance (ANOVA) followed by Tukey–Kramer multiple comparisons was used to analyze the data. A value of  $P < 0.05$  was considered as the significance level between the groups.

#### Acknowledgments

Financial support of this project by Iranian National Science Foundation (INSF) is acknowledged. Authors also thank the support of the Vice-chancellor of Research of Shiraz University of Medical Sciences (Grant number: 5001).

#### References and notes

1. Carter, M. D.; Simms, G. A.; Weaver, D. F. *Clin. Pharmacol. Ther.* **2010**, *88*, 475.

2. Verdon, C. M.; Fossati, P.; Verny, M.; Dieudonne, B.; Teillet, L.; Nadel, J. *Alz. Dis. Assoc. Dis.* **2007**, *21*, 25.
3. Silvestri, R. *Med. Res. Rev.* **2009**, *29*, 295.
4. Vassar, R. *Adv. Drug Deliver. Rev.* **2002**, *54*, 1589.
5. Sinha, S.; Anderson, J. P.; Barbour, R.; Basi, G. S.; Caccavello, R.; Davis, D.; Doan, M.; Dovey, H. F.; Frigon, N.; Hong, J. *Nature* **1999**, *402*, 537.
6. Vassar, R.; Bennett, B. D.; Babu-Khan, S.; Kahn, S.; Mendiaz, E. A.; Denis, P.; Teplow, D. B.; Ross, S.; Amarante, P.; Loeloff, R. *Science* **1999**, *286*, 735.
7. Selkoe, D. J. *J. Biol. Chem.* **1996**, *271*, 18295.
8. Huang, W. H.; Sheng, R.; Hu, Y. Z. *Curr. Med. Chem.* **1806**, *2009*, 16.
9. Creed, M. C.; Milgram, N. W. *Age* **2010**, *32*, 365.
10. Luo, Y.; Bolon, B.; Kahn, S.; Bennett, B. D.; Babu-Khan, S.; Denis, P.; Fan, W.; Kha, H.; Zhang, J.; Gong, Y. *Nat. Neurosci.* **2001**, *2001*, 4.
11. Ghosh, A. K.; Brindisi, M.; Tang, J. J. *Neurochem.* **2012**, *1*, 71.
12. Albert, J. S. *Prog. Med. Chem.* **2009**, *48*, 133.
13. Ziora, Z.; Kimura, T.; Kiso, Y. *Drugs Future* **2006**, *31*, 53.
14. Stachel, S. J. *Drug Develop. Res.* **2009**, *70*, 101.
15. Niu, Y.; Gao, H.; Xu, F.; Wang, C.; Liu, P.; Yang, G.; Sun, Q.; Xu, P. *Chem. Biol. Drug Des.* **2012**, *80*, 775.
16. Gaulton, A.; Bellis, L. J.; Bento, A. P.; Chambers, J.; Davies, M.; Hersey, A.; Light, Y.; McGlinchey, S.; Michalovich, D.; Al-Lazikani, B. *Nucleic Acids Res.* **2012**, *40*, D1100.
17. Miri, R.; Javidnia, K.; Mirkhani, H.; Kazemi, F.; Hemmateenejad, B.; Edraki, N.; Mehdipour, A. R. *DARU* **2008**, *16*, 263.
18. Kumar, R. S.; Idhayadhulla, A.; Abdul Nasser, A. J.; Selvin, J. *Eur. J. Med. Chem.* **2011**, *46*, 804.
19. Choi, S. J.; Cho, J. H.; Im, I.; Lee, S. D.; Jang, J. Y.; Oh, Y. M.; Jung, Y. K.; Jeon, E. S.; Kim, Y. C. *Eur. J. Med. Chem.* **2010**, *45*, 2578.
20. Al-Nadaf, A.; Abu Sheikha, G.; Taha, M. O. *Bioorg. Med. Chem.* **2010**, *1*, 9.
21. Bodor, N.; Buchwald, P. *Adv. Drug Deliver. Rev.* **1999**, *36*, 229.
22. Bodor, N.; Buchwald, P. *Drug Discovery Today* **2002**, *7*, 766.
23. Wang, P.; Song, L.; Yi, H.; Zhang, M.; Zhu, S.; Deng, H.; Shao, M. *Tetrahedron Lett.* **2010**, *51*, 3975.
24. Edraki, N.; Firuzi, O.; Foroumadi, A.; Miri, R.; Madadkar-Sobhani, A.; Khoshneviszadeh, M.; Shafiee, A. *Bioorg. Med. Chem.* **2013**, *21*, 2396.
25. Miri, R.; Motamedi, R.; Rezaei, M. R.; Firuzi, O.; Javidnia, A.; Shafiee, A. *Archiv der Pharmazie.* **2010**, *1*, 111.
26. Miri, R.; Firuzi, O.; Peymani, P.; Zamani, M.; Mehdipour, A. R.; Heydari, Z.; Masteri Farahani, M.; Shafiee, A. *Chem. Biol. Drug Des.* **2012**, *79*, 68.
27. Putta, S.; Beroza, P. *Curr. Top. Med. Chem.* **2007**, *7*, 1514.
28. Laurie, R.; Alasdair, T.; Jackson, R. M. *Curr. Protein Pept. Sci.* **2006**, *7*, 395.
29. Jorgensen, W. *Science* **2004**, *303*.
30. Sellers, R. P.; Alexander, L. D.; Johnson, V. A.; Lin, C. C.; Savage, J.; Corral, R.; Moss, J.; Slugocki, T. S.; Singh, E. K.; Davis, M. R. *Bioorg. Med. Chem. Lett.* **2010**, *18*, 6822.
31. Hevener, K. E.; Zhao, W.; Ball, D. M.; Babaoglu, K.; Qi, J.; White, S. W.; Lee, R. E. *J. Chem. Inf. Model.* **2009**, *49*, 444.
32. Ghorban Dadrass, L.; Madadkar Sobhani, A.; Shafiee, A.; Mahmoudian, M. *DARU* **2004**, *12*, 1.
33. Gevariya, H.; Desai, B.; Vora, V.; Shah, A. *Heterocycl. Commun.* **2001**, *5*, 481.
34. Razzaghi-Asl, N.; Ebadi, A.; Edraki, N.; Shahabipour, S.; Miri, R. *Med. Chem. Res.* **2013**, *22*, 3259.
35. Stachel, S. J.; Coburn, C. A.; Steele, T. G.; Crouthamel, M. C.; Pietrak, B. L.; Lai, M. T.; Holloway, M. K.; Munshi, S. K.; Grahama, S. L.; Vacca, J. P. *Bioorg. Med. Chem. Lett.* **2006**, *16*, 641.
36. Klamt, A.; Schüürmann, G. *J. Chem. Soc., Perkin Trans. 2* **1993**, 799.
37. Viswanath, I. V. K.; Murphy, Y. L. N. *Chem. Sci. Trans.* **2013**, *2*, 227.
38. Lakshmi Kantam, M.; Mahendar, K.; Bhargava, S. *J. Chem. Sci.* **2010**, *122*, 63.
39. Yang, S. H.; Zhao, F. Y.; Lu, H. Y.; Deng, J.; Zhang, Z. H. *J. Heterocycl. Chem.* **2012**, *49*, 1126.
40. Moitessier, N.; Therrien, E.; Hanessian, S. *J. Med. Chem.* **2006**, *49*, 5885.
41. Kuglstatter, A.; Stahl, M.; Peters, J. U.; Huber, W.; Stihle, M.; Schlatter, D.; Benz, J.; Ruf, A.; Roth, D.; Enderle, T.; Hennig, M. *Bioorg. Med. Chem. Lett.* **2008**, *18*, 1304.
42. Morris, G. M.; Huey, R.; Lindstrom, W.; Sanner, M. F.; Belew, R. K.; Goodsell, D. S.; Olson, A. J. *J. Comput. Chem.* **2009**, *30*, 2785.
43. Van Der Spoel, D.; Lindahl, E.; Hess, B.; Groenhof, G.; Mark, A. E.; Berendsen, H. J. C. *J. Comput. Chem.* **2005**, *26*, 1701.
44. Wallace, A. C.; Laskowski, R. A.; Thornton, J. M. *Protein Eng.* **1995**, *8*, 127.
45. Fogarasi, G.; Zhou, X.; Taylor, P. W.; Pulay, P. *J. Am. Chem. Soc.* **1992**, *114*, 8191.
46. Bykov, D.; Neese, F. *J. Biol. Inorg. Chem.* **2011**, *16*, 417.
47. Bykov, D.; Neese, F. *J. Biol. Inorg. Chem.* **2012**, *17*, 741.
48. Neese, F.; University of Bonn, 2011.
49. Jain, T. K.; Morales, M. A.; Sahoo, S. K.; Leslie-Pelecky, D. L.; Labhasetwar, V. *Mol. Pharm.* **2005**, *2*, 194.
50. Clemens, R. J.; Hyatt, J. A. *J. Org. Chem.* **1985**, *50*, 2431.
51. Mohammadi-Samani, S.; Miri, R.; Salmanpour, M.; Khalighian, N.; Sotoudeh, S.; Erfani, N. *RPS* **2013**, *8*, 25.